Author's Choice

THE JOURNAL OF BIOLOGICAL CHEMISTRY VOL. 286, NO. 34, pp. 29848–29860, August 26, 2011

Cell Type-specific Target Selection by Combinatorial Binding of Smad2/3 Proteins and Hepatocyte Nuclear Factor 4α in HepG2 Cells*[S]◆

Received for publication, December 30, 2010, and in revised form, May 19, 2011 Published, JBC Papers in Press, June 6, 2011, DOI 10.1074/jbc.M110.217745

Anna Mizutani[‡1], Daizo Koinuma[‡], Shuichi Tsutsumi[§], Naoko Kamimura[§], Masato Morikawa[‡], Hiroshi I. Suzuki[‡], Takeshi Imamura[¶2], Kohei Miyazono[‡3], and Hiroyuki Aburatani[§]

From the [‡]Department of Molecular Pathology, Graduate School of Medicine, University of Tokyo, Bunkyo-ku, Tokyo 113-0033, the [§]Genome Science Division, Research Center for Advanced Science and Technology, University of Tokyo, Meguro-ku, Tokyo 153-8904, and the [¶]Division of Biochemistry, Cancer Institute of the Japanese Foundation for Cancer Research, Koto-ku, Tokyo 135-8550, Japan

Specific regulation of target genes by transforming growth factor-β (TGF-β) in a given cellular context is determined in part by transcription factors and cofactors that interact with the Smad complex. In this study, we determined Smad2 and Smad3 (Smad2/3) binding regions in the promoters of known genes in HepG2 hepatoblastoma cells, and we compared them with those in HaCaT epidermal keratinocytes to elucidate the mechanisms of cell type- and context-dependent regulation of transcription induced by TGF-β. Our results show that 81% of the Smad2/3 binding regions in HepG2 cells were not shared with those found in HaCaT cells. Hepatocyte nuclear factor 4α (HNF4α) is expressed in HepG2 cells but not in HaCaT cells, and the HNF4α-binding motif was identified as an enriched motif in the HepG2-specific Smad2/3 binding regions. Chromatin immunoprecipitation sequencing analysis of HNF4α binding regions under TGF-β stimulation revealed that 32.5% of the Smad2/3 binding regions overlapped HNF4α bindings. *MIXL1* was identified as a new combinatorial target of HNF4α and Smad2/3, and both the HNF4α protein and its binding motif were required for the induction of *MIXL1* by TGF-β in HepG2 cells. These findings generalize the importance of binding of HNF4α on Smad2/3 binding genomic regions for HepG2-specific regulation of transcription by TGF-β and suggest that certain transcription factors expressed in a cell type-specific manner play important roles in the transcription regulated by the TGF-β-Smad signaling pathway.

Transforming growth factor-β (TGF-β) has multiple roles in growth arrest, apoptosis, differentiation, epithelial-to-mesenchymal transition, and extracellular matrix deposition in various types of cells and is related to embryonic development and various human diseases (1). In cancer cells, TGF-β is known to possess conflicting tumor-suppressive and pro-metastatic functions; TGF-β inhibits cancer progression by cell cycle arrest and apoptosis, although it also helps cancer cells to evade anti-tumor immune response and metastasize to distant organs by epithelial-to-mesenchymal transition. Understanding the precise regulatory mechanisms downstream of this signaling pathway is required for the control of diseases.

Smad family proteins are the principal and specific molecules that transduce signals from the ligand-bound active receptor complexes on the cell surface membrane to the nucleus (2–4). Smad2 and Smad3 form hetero-oligomers with Smad4 after phosphorylation of the C terminus of Smad2 or Smad3 by the receptor complex, and the Smad complex serves as a transcription factor on the genome. The Smad complex was reported to bind to the sequences containing "GTCT" (Smad-binding element) by *in vitro* screening of the binding sequences and structural analysis of the Smad complex bound to the DNA (5, 6). However, this very simple motif is present everywhere in the genome. It has also been suggested that the binding affinity of the Smad complex to Smad-binding elements is not high. Interaction with other transcription factors and cofactors has been shown to be important to provide functional specificity of TGF-β signaling, and these transcription factors and cofactors facilitate binding of the Smad complex to the favorable positions in the genome. Expressions of these transcription factors and cofactors are often regulated in a cell- or tissue-specific manner, and a subset of these molecules indeed has been shown to be important for the context-dependent Smad binding to the genome and transcriptional regulation of target genes. Target genes of TGF-β that are regulated by the same cofactors are designated as a synexpression group (7), as reported in the regulation of several genes such as *CDKN1A/p21* and *GADD45A* by FOXO family proteins (8).

High throughput analyses of transcription factor binding regions using either an oligonucleotide tiling microarray or massively parallel sequencing are now widely used to understand the roles of transcription factors (9, 10). We have identi-

* This work was supported by KAKENHI Grant-in-Aid for Scientific Research on Innovative Areas, Integrative Research on Cancer Microenvironment Network, 22112002 (to K. M.) Grants-in-Aid for Scientific Research (S) 20221009 (to H. A.) and for Young Scientists (B) 10014456 (to D. K.) from the Ministry of Education, Culture, Sports, Science, and Technology of Japan, a grant from the Genome Network Project from Ministry of Education, Culture, Sports, Science, and Technology of Japan (to H. A.), and the Global Center of Excellence Program (Integrative Life Science Based on the Study of Biosignaling Mechanisms) from the Japan Society for the Promotion of Science.

◆ This article was selected as a Paper of the Week.

Author's Choice—Final version full access.

[S] The on-line version of this article (available at http://www.jbc.org) contains supplemental Figs. S1 and S2 and Tables S1–S6.

[1] Supported by an Ishidsu Shun Memorial Scholarship.

[2] Present address: Dept. of Molecular Medicine for Pathogenesis, Ehime University Graduate School of Medicine, Toon, Ehime 791-0295, Japan.

[3] To whom correspondence should be addressed. Tel.: 81-3-5841-3356; Fax: 81-3-5841-3354; E-mail: miyazono@m.u-tokyo.ac.jp.

fied Smad2/3 binding regions and Smad4 binding regions using a promoter tiling array in the HaCaT normal human epidermal keratinocyte cell line (11, 12). We found Smad2/3 binding regions at the previously analyzed regions as well as many unrecognized binding regions. Activator protein-1 (AP-1), v-Ets erythroblastosis virus E26 oncogene homolog, and transcription factor AP-2-binding motifs were identified as enriched motifs in the Smad2/3 binding regions in HaCaT cells (11). However, it remains to be determined whether the identified Smad2/3 binding regions are shared with those in other cells and tissues.

Hepatocyte nuclear factor 4α (HNF4α)[4] is a member of the hepatocyte nuclear factor family, which includes well conserved nuclear receptors among mammals. HNF4α is expressed in the liver, kidney, small intestine, and pancreas and is essential for the organogenesis of the liver (13, 14). HNF4α is also required for the differentiation of hepatocytes and is engaged in hepatocyte-specific gene regulation related to the synthesis of apolipoproteins, acute phase reactive proteins, and other secreted proteins. HNF4α is located in the nucleus, forms a homodimer, and functions as a transcription factor by binding to DR1 elements in the genome (15).

Several groups have identified a functional relationship between HNF4α and TGF-β signaling. TGF-β down-regulates the expression of variant 1 of HNF4α, one of the transcriptional variants of HNF4α, which has an AF1 transcriptional activation domain in their N terminus (16). On the contrary, the expression of the transcriptional activation domain lacking variant 8 is repressed by TGF-β in normal murine mammary gland (NMuMG) epithelial cells (17). TGF-β has also been reported to regulate the HNF4α expression by proteasome-dependent degradation (16). The effect of HNF4α on TGF-β-induced transcription has also been analyzed for the *APOC3* promoter, where HNF4α interacts with Smad3 and Smad4 to induce the *APOC3* expression (18, 19). The HNF4α-binding motif in the *APOC3* promoter has been shown to be important for TGF-β-induced transcriptional activity, and a mutant of Smad3 that lacks the DNA binding property to Smad-binding elements still interacts with HNF4α to synergistically transactivate the *APOC3* promoter (19). Because HNF4α binds to the MH1 DNA binding domain of Smad3 through both its N and C termini (19), Smads may indirectly bind to the *APOC3* promoter through HNF4α. However, it is still unclear whether the reported interaction with Smads and mechanisms of transcriptional regulation are generally important for the function of both HNF4α and Smads in hepatocytes.

Here, we identified Smad2/3 binding regions in the HepG2 hepatoblastoma cell line and compared them with the binding regions in HaCaT cells and hepatocellular carcinoma Hep3B cells to elucidate the mechanisms of context-dependent regulation of TGF-β-induced transcription. We found HNF4α as an important factor for HepG2-specific Smad2/3 binding regions and analyzed its regulatory mechanism using a new target gene of HNF4α, *MIXL1*, under TGF-β stimulation.

[4] The abbreviations used are: HNF4α, hepatocyte nuclear factor 4α; qPCR, quantitative PCR; ChIP-seq, ChIP sequencing; FDR, false discovery rate; CEAS, cis-regulatory element annotation system.

EXPERIMENTAL PROCEDURES

Cell Culture—Human hepatoblastoma HepG2 cells and hepatocellular carcinoma Hep3B cells were obtained from the American Type Culture Collection and were cultured in minimum essential medium (Invitrogen) supplemented with 10% fetal bovine serum (FBS) (Thermo Scientific, Rockford, IL), 0.1 mM nonessential amino acids, 1 mM sodium pyruvate, 100 units/ml penicillin G, and 100 μg/ml streptomycin. HaCaT cells were maintained in Dulbecco's modified Eagle's medium (DMEM; catalog no. 11965; Invitrogen) supplemented with 10% FBS, 100 units/ml penicillin G, and 100 μg/ml streptomycin. Cells were grown in a humidified atmosphere with 5% CO_2 at 37 °C.

Antibodies and Chemicals—We used the following commercially available antibodies: mouse anti-Smad2/3 (BD Biosciences), anti-α-tubulin (DM1A) (Sigma), rabbit anti-phospho-Smad2 (Cell Signaling Technology, Beverly, MA), anti-phospho-Smad3 (Cell Signaling Technology), and anti-HNF4α (Santa Cruz Biotechnology, Santa Cruz, CA). TGF-β3 was from R & D Systems (Minneapolis, MN).

RNA Interference and Oligonucleotides—Stealth small interfering RNA (siRNA) targeting HNF4α (5′-AAAGCGGCCACGCGAGUCAUACUGG-3′) was purchased from Invitrogen. As a negative control, we used a predesigned siRNA (12935–200, sequence not available). siRNAs were introduced into HepG2 cells using the Lipofectamine RNAi MAX reagent (Invitrogen) according to the manufacturer's instructions (reverse transfection method), using 3 nM siRNA per 1×10^5 cells/ml per well of 12-well plates.

Immunoblotting—SDS-gel electrophoresis and immunoblotting were performed as described, using a LAS-4000 lumino-image analyzer (Fujifilm, Tokyo, Japan) (20). RIPA buffer (1% Nonidet P-40, 0.5% sodium deoxycholate, 0.1% SDS, 150 mM NaCl, 50 mM Tris-HCl (pH 8.0), 5 mM EDTA) was used for cell lysis.

Chromatin Immunoprecipitation (ChIP), ChIP-chip, and ChIP Sequencing (Seq)—Sample preparation for ChIP-chip analysis was performed as described previously, using anti-Smad2/3 (BD Biosciences) (11, 21, 22). Briefly, ChIP and control input DNA samples were amplified by two cycles of *in vitro* transcription and hybridized on separate Affymetrix human promoter 1.0R oligonucleotide tiling arrays (Affymetrix, Santa Clara, CA). Enrichment values (ChIP/control input DNA) were calculated using the MAT algorithm, and Smad2/3 binding regions were determined using detection p values of 10^{-4} (23). For conventional quantitative anti-Smad2/3 ChIP-quantitative PCR (ChIP-qPCR) analyses, cells were cross-linked with 10 mM dimethyl adipimidate (Thermo Scientific) for 30 min at room temperature before formaldehyde fixation. Bioruptor UCW-301 (output: H, 2 cycles of 30 s of sonication with 30-s intervals; Cosmobio, Tokyo, Japan) was used for sonication of ChIP-qPCR samples. Sample preparation for ChIP-seq was performed according to the manufacturer's instructions (Illumina, San Diego). The obtained read tags were mapped on the NCBI/hg18 human genome assembly using ELAND (Illumina). Cis-Genome was used for the calculation of significant HNF4α

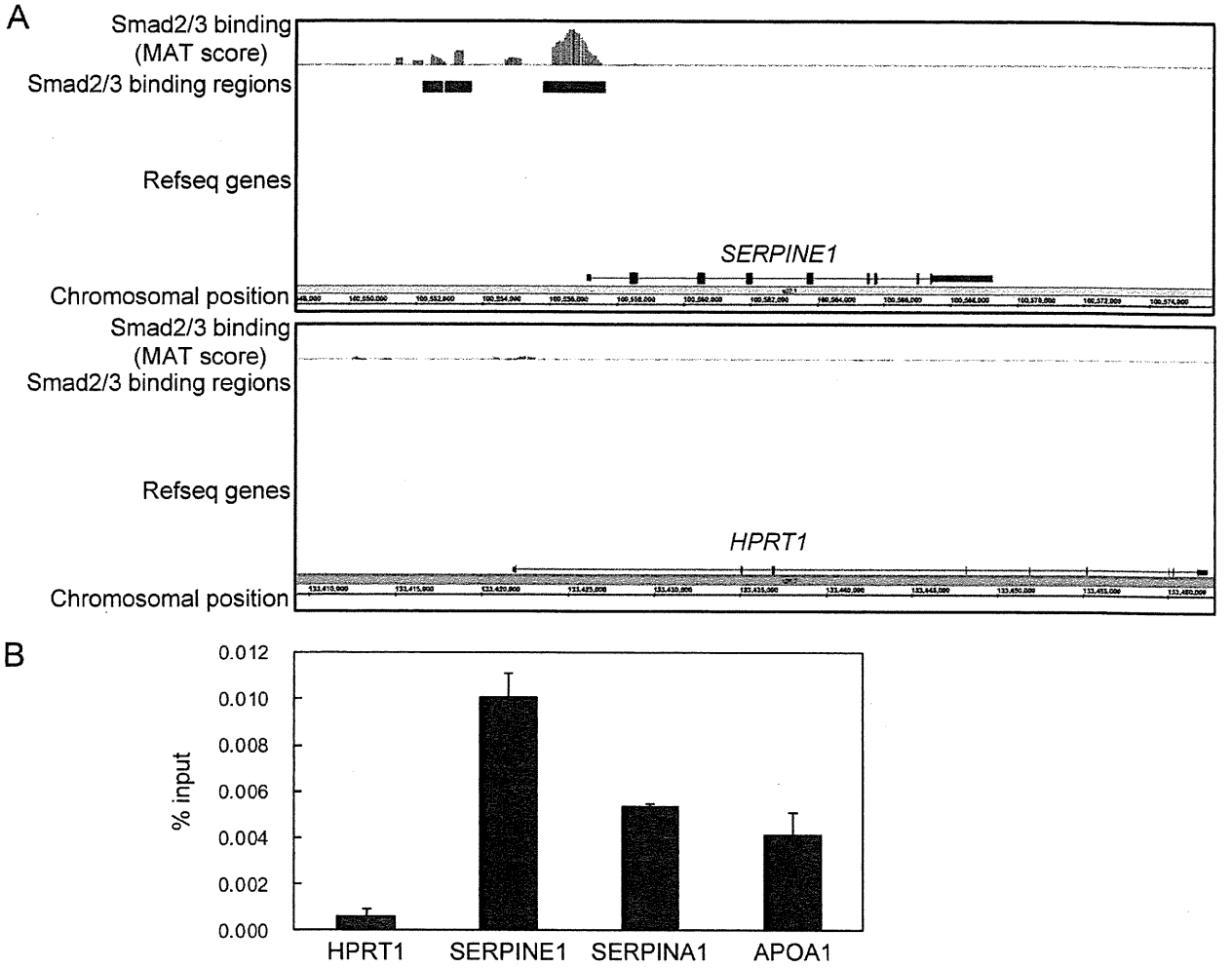

FIGURE 1. **Identification of Smad2/3 binding regions in HepG2 cells.** *A*, Smad2/3 binding to the *SERPINE1/PAI-1* locus in HepG2 cells. MAT scores were plotted at the *SERPINE1* and *HPRT1* loci to obtain a graphical representation of Smad2/3 binding in these regions. Significant Smad2/3 binding regions as determined by detection of *p* values of 10^{-4} are shown by *black bars*. *B*, percent input values of Smad2/3 binding compared with input genome as determined by ChIP-qPCR. Cells were treated with 120 pM TGF-β for 1.5 h. Cells were cross-linked sequentially with dimethyl adipimidate and formaldehyde. *Error bars* represent S.D.

binding regions (one-sample analysis, with default parameters and a false discovery rate (FDR) of less than 0.1%) (24).

Motif Prediction and Mapping—CisGenome was used for both *de novo* motif prediction and motif mapping of Smad2/3 ChIP-chip and HNF4α ChIP-seq binding regions. Cis-regulatory element annotation system (CEAS) was also used for identification of known motifs in Smad2/3 and HNF4α binding regions (25).

Quantitative PCR Analysis—Quantitative real time PCR analysis was performed as described previously (26). Amplification data were quantified using the standard curve method. Detected signals were confirmed to be specific by a dissociation protocol. All samples were run in duplicate or triplicate, and the results were averaged. Sequences of the primers are available in supplemental Tables S1 and S2.

Reverse Transcription-PCR and Expression Microarray Analysis—Total RNAs were extracted as described previously (26). First strand cDNAs were synthesized using the PrimeScript2 reverse transcriptase (TakaraBio, Shiga, Japan). The experimental procedures for GeneChip (Affymetrix) were performed as described previously (11) using the GeneChip human U133 plus 2.0 oligonucleotide array (Affymetrix). Microarray Suite software 5.0 (Affymetrix) was used with a target intensity of 100. Data from one array were obtained for each sample.

Promoter Reporter Constructs and cDNA Constructs—The human *MIXL1* promoter reporter (MIXL1-WT-luc, −583 to −8) and its mutants were constructed by a PCR-based approach and cloned into the pGL4.10 (Promega, Fitchburg, WI) vector with a minimal luciferase promoter sequence (11). Primer sequences used for the construction of MIXL1-mut1-luc were 5′-GCAGGGGTGGTAAATAAATTTAGGGTTATCGGGACAGACGGGAC-3′ and 5′-GTCCCGTCTGTCCGATAACCCTAAATTTATTTACCACCCCTGC-3′. The primer sequences for the construction of MIXL1-mut2-luc were 5′-TCCCCGAGCCCTTAGGGTATTACACCGCCCCGCCTTC-3′ and 5′-GAAGGCGGGGCGGTGTAATACCCTAAGGGCTCGGGGA-3′. MIXL1-luc reporters with mutations in Smad-binding elements were also constructed by

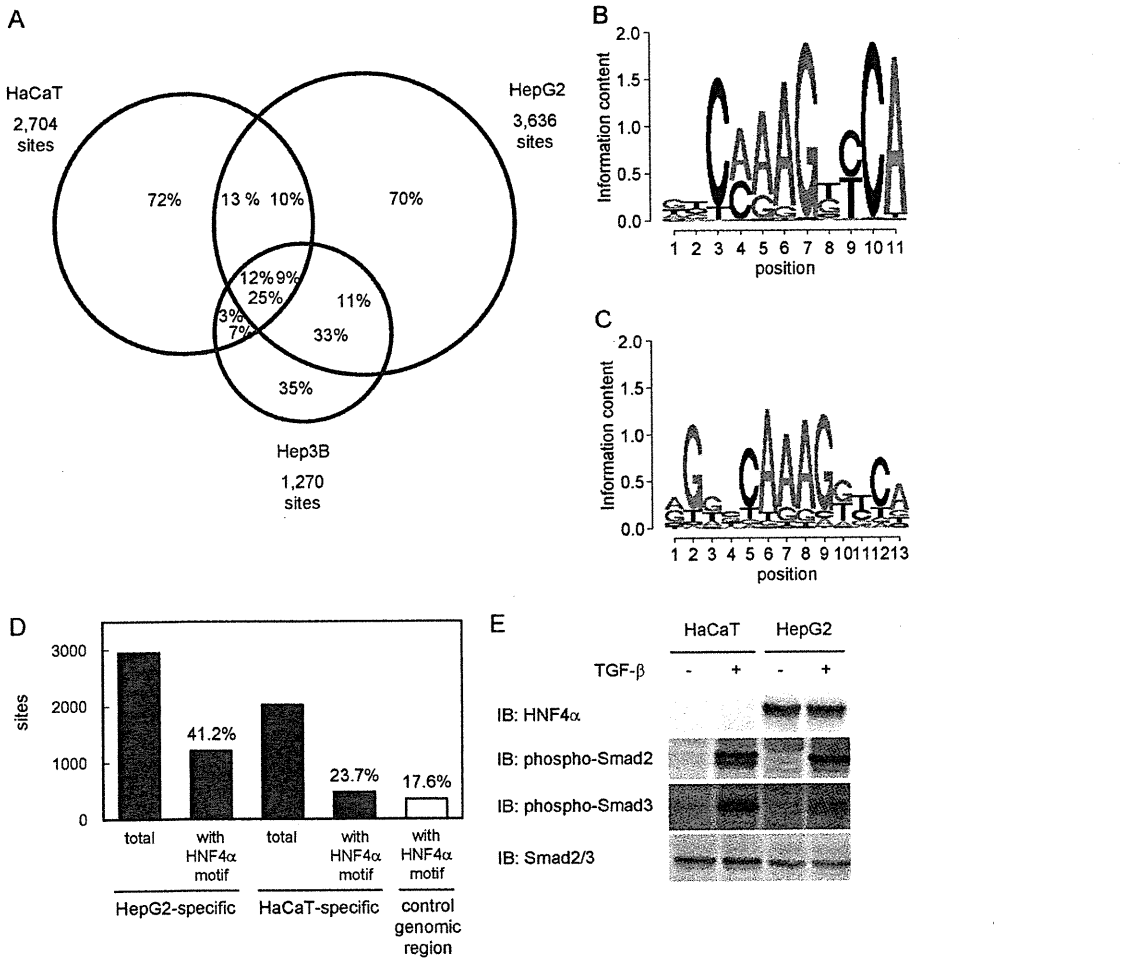

FIGURE 2. **Comparison of the Smad2/3 binding regions among different cell lines.** *A*, Venn diagrams showing the overlaps of Smad2/3 binding regions in HaCaT, HepG2, and Hep3B cells. *Numbers* in the *circles* indicate percentages of the Smad2/3 binding region of each cell line (*red*, HaCaT; *black*, HepG2; *blue*, Hep3B). *B*, identification of a motif conserved in HepG2-specific Smad binding regions. Partial genomic sequences within 250 bp from the peak positions of HepG2-specific Smad2/3 binding regions (n = 2,955) were analyzed using the CisGenome Gibbs motif sampler. Default parameters were used for the calculation, except for the numbers of motifs to be identified (n = 10). Matrix datum of the motif calculated by CisGenome was graphically shown using the SegLogo function of the R software. *C*, HNF4α-binding motif that matched the predicted motif in HepG2-specific Smad2/3 binding regions. The JASPAR CORE data base was used to identify known transcription factor binding motifs similar to the calculated matrix data in *B*. An HNF4α motif (ID: MA0114.1) was identified as the most similar motif with a comparison score of 21.3, which reached 96.9% of the potential maximal score. *D*, frequencies of the HNF4α-binding motif in Smad2/3 binding regions. Presence of the HNF4α-binding motif in each Smad2/3 binding region (within 250 bp from the peak signal position) was determined using CisGenome. Frequencies of the motif in either HepG2- or HaCaT-specific Smad2/3 binding regions were then calculated. As a control, matched genomic regions to HaCaT-specific Smad2/3 binding regions were obtained using CisGenome, and the frequency of the HNF4α motif was determined. *E*, expression of the HNF4α protein and phosphorylation of Smad2/3 in HaCaT and HepG2 cells. Cells were treated with TGF-β for 1.5 h, and the expression of each protein was determined by immunoblotting (*IB*).

PCR (see Fig. 6*D* for sequences of the mutants). HNF4α and its C115R mutant were constructed by a PCR-based approach using the first strand cDNA of HepG2 cells as a template. The sequences of all cDNAs constructed were verified by sequencing.

Luciferase Assay—Cells in 24-well plates were transfected with different combinations of promoter reporter constructs and expression plasmids by using Lipofectamine LTX (Invitrogen). The total amount of transfected DNA was adjusted to the same amount using an empty vector. Twenty four hours later, cells were treated with TGF-β for an additional 24–48 h and lysed. Luciferase activities in the lysates were measured using the Dual-Luciferase® reporter system (Promega) as described previously. For normalization, cells were co-transfected with pGL4.75-SV40-hRluc. Where indicated, siRNAs were transfected 24 h before reporter transfection. All samples were prepared in triplicate, and results were averaged.

Statistical Analysis—The Tukey-Kramer test of R program was used for multiple comparisons of data. The t test was used for two-sample analysis. p values of less than 0.05 were considered to indicate significance for each experiment.

RESULTS

Identification of HNF4α-binding Motif in HepG2-specific Smad2/3 Binding Regions—To determine Smad2/3 binding regions in HepG2 hepatoblastoma cells, we stimulated the cells with TGF-β for 1.5 h and fixed them with formaldehyde to cross-link genome-bound molecules to DNA. ChIP on microarray analysis (ChIP-chip) was performed according to the established protocol using an Affymetrix human promoter

array (22). Obtained image data were analyzed using the MAT algorithm, which provided enrichment values of the ChIP samples for every promoter region, compared with the input genomic sample. There was significant Smad2/3 binding to the promoter region of the *SERPINE1/PAI-1* gene as observed previously in the ChIP-chip analysis of Smad2/3 bindings in HaCaT cells (Fig. 1*A*, *upper panel*) (11). In contrast, there was no significant Smad2/3 binding to the *HPRT1* locus that served

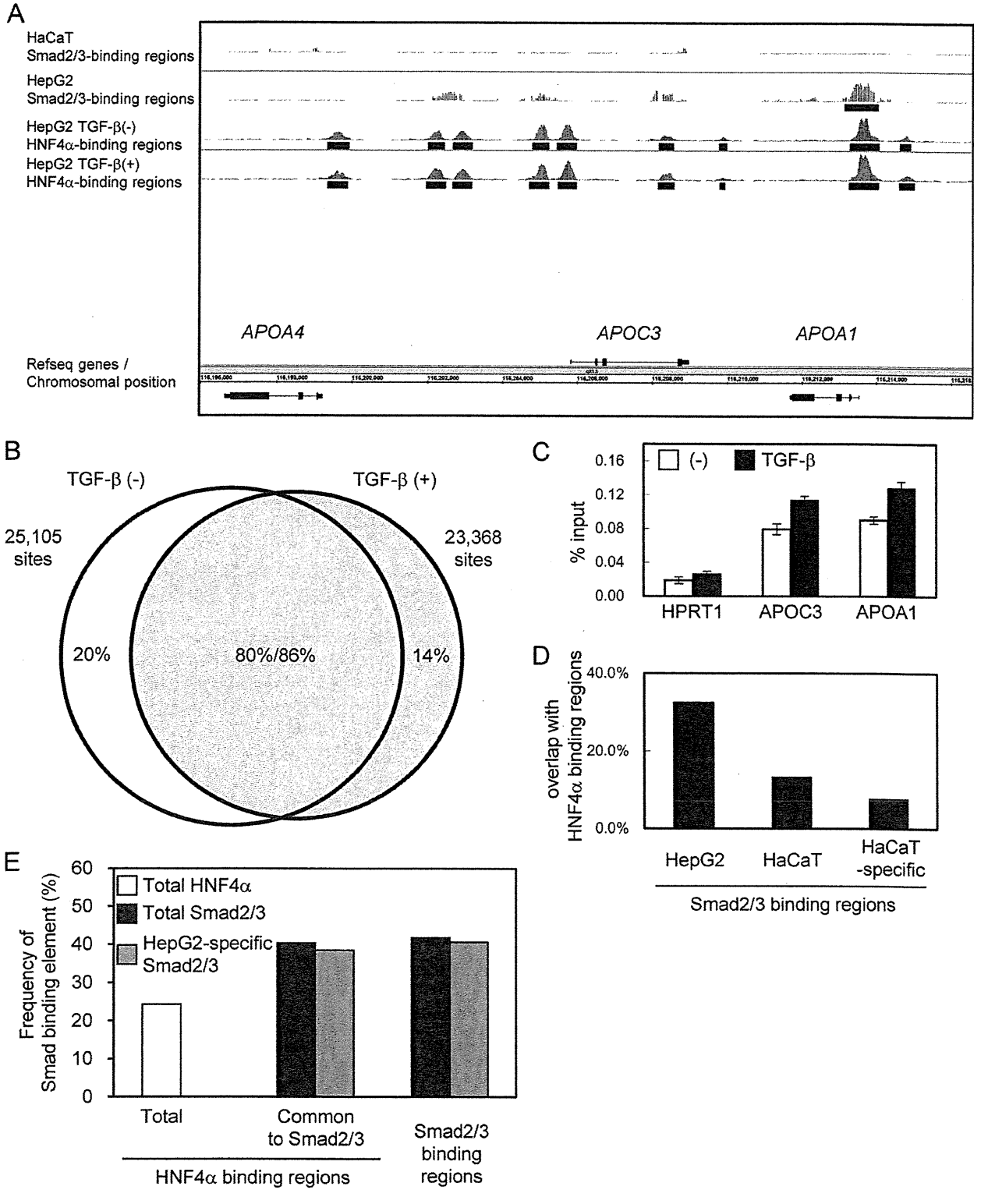

as a negative control region (Fig. 1*A*, *lower panel*). We confirmed significant enrichment of Smad2/3 binding to the *SERPINE1*, *SERPINA1*/α-antitrypsin, and *APOA1* loci using ChIP-qPCR (Fig. 1*B*). We identified 3,636 significant Smad2/3 binding regions that had detection p values of less than 10^{-4} within the promoter regions of known genes.

Next, we compared the identified Smad2/3 binding regions in HepG2 cells to those in HaCaT cells (11). We also obtained 1,270 Smad2/3 binding regions in Hep3B hepatocellular carcinoma cells to determine their overlaps (Fig. 2*A*). We found that only 25.2% of the Smad2/3 binding regions in HaCaT cells (n = 682) were shared with those in HepG2 cells. In contrast, 58.3% of the binding regions in Hep3B cells overlapped with those identified in HepG2 cells, although the number of overlapping binding regions (n = 741) was similar to that between HaCaT and HepG2 cells. Many of the Smad2/3 binding regions were thus unique to each cell type. We determined the candidate target genes of Smad2/3 using the dataset of Smad2/3 binding regions that were either common to HepG2 and HaCaT, HepG2-specific, or HaCaT-specific (supplemental Tables S3-S5), and performed gene ontology analysis of each category by DAVID (27). We did not observe remarkable differences in the top five enriched annotation clusters between the common Smad2/3 binding regions and HepG2-specific Smad2/3 binding region. Conversely, enrichment of cell death and cytoskeleton-related annotations was found in HaCaT-specific binding regions (supplemental Table S6).

To identify specific motifs in the Smad2/3 binding regions in HepG2 cells, *de novo* motif prediction was performed using the CisGenome Gibbs motif sampler (supplemental Fig. S1*A*). We searched for known motifs that had similarity to the calculated motifs using the JASPAR data base (28). As shown in Fig. 2*C*, we found that one predicted motif (Fig. 2*B*) was strongly similar to the HNF4α-binding motif (Fig. 2*C*, 96.9% score). The frequency of the HNF4α motif in HepG2-specific Smad2/3 binding regions was 41.2%, although that in HaCaT-specific Smad2/3 binding regions and its matched random genomic regions was 23.7 and 17.6%, respectively (Fig. 2*D*). We also analyzed the sequences in Smad2/3 binding regions using the CEAS analysis tool as we did in our previous report (11, 12, 25), and the HNF4α-binding motif was identified as one of the top three enriched motifs in the binding sequences (supplemental Fig. S1*B*) (25). It should be noted that canonical Smad-binding element (M00974.SMAD, "CAGAC") was also identified as enriched motif through CEAS analysis and present in 40.6% of the HepG2-specific Smad2/3 binding regions (data not shown). These findings suggested that the HNF4α motif was enriched in HepG2-specific Smad2/3 binding regions and had roles for cell type specificity of Smad2/3 binding and TGF-β-induced transcription in HepG2 cells. HNF4α is one of the "master genes" of hepatocytes and is essential for hepatocyte-specific gene expressions and functions. Because HNF4α was not expressed in HaCaT cells (Fig. 2*E*), we decided to determine HNF4α binding regions *in vivo* in the presence of TGF-β.

HNF4α Binding to Its Binding Regions Is Not Extensively Altered by TGF-β—ChIP-chip and ChIP-seq studies of HNF4α binding regions have been reported using HepG2 cells (29–31). We retrieved data (30) from the data base and found that 20.7% of the Smad2/3 binding regions were common to HNF4α binding regions *in vivo*. However, no reports have yet determined the changes in the binding of HNF4α by extracellular stimulations, including that by TGF-β. We therefore acquired the HNF4α binding data using the newly available ChIP-seq technology to compare the Smad2/3 binding with the HNF4α binding under TGF-β stimulation. We identified 25,105 significant HNF4α binding regions in the absence of TGF-β and 23,368 regions in the presence of TGF-β, at an FDR of less than 0.1%. The *APOA4/APOC3/APOA1* gene cluster that is a known target of HNF4α is shown in Fig. 3*A*. We observed significant HNF4α binding to several of these regions in the absence of TGF-β, and the binding was not extensively changed following stimulation. We also found that there was significant Smad2/3 binding to the *APOA1* promoter, which was absent in HaCaT cells. Our data showed that Smad2/3 binding to the *APOC3* promoter was not significant.

We then examined the changes in HNF4α binding by TGF-β stimulation. More than 80% of the HNF4α binding regions overlapped between TGF-β-treated and untreated cells. However, there were also specific binding regions for both TGF-β-treated and untreated cells (Fig. 3*B*). In addition, we calculated the changes in the normalized read numbers within the HNF4α binding regions by TGF-β stimulation and found that some regions indeed had either decreased or increased sequence reads following TGF-β stimulation (data not shown). Percent input values of HNF4α binding to the *APOC3* and *APOA1* loci were also up-regulated to some extent (Fig. 3*C*), suggesting that there were some, if limited, roles of TGF-β for HNF4α binding. Using the HNF4α binding data with TGF-β stimulation, we determined the frequency of HNF4α binding in Smad2/3 binding regions *in vivo*. We found that 32.5% of the Smad2/3 binding regions in HepG2 cells were indeed common to HNF4α binding regions. In contrast, only 13.2% of Smad2/3 binding regions in HaCaT cells were common, and the frequency decreased to 7.7% when HaCaT-specific Smad2/3 binding regions were examined (Fig. 3*D*). These results suggested that HNF4α and Smad2/3 binding regions are located in close prox-

FIGURE 3. **Identification of HNF4α binding regions in the presence and absence of TGF-β stimulation.** *A*, graphical representation of HNF4α binding to the *APOA4/APOC3/APOA1* gene loci. Sequence read numbers of 100-bp sliding window were plotted for HNF4α ChIP-seq samples. Smad2/3 bindings as determined by ChIP-chip analysis were shown in the *upper two panels* as in Fig. 1*A*. *Black bars* represent significant binding regions (FDR, <0.1%). *B*, Venn diagrams showing overlap between TGF-β-treated and untreated HNF4α binding regions. HNF4α binding regions were determined for each sample (FDR, <0.1%). HNF4α binding regions that have overlapping regions within 500 bp from their positions of maximum read numbers were considered as shared binding regions. *C*, changes in the HNF4α binding to *APOC3* and *APOA1* loci were quantitatively determined by ChIP-qPCR analysis. *Error bars*, S.D. *D*, frequencies of *in vivo* HNF4α binding to the Smad2/3 binding regions. Percentages of HNF4α binding within 250 bp from the peak signal position of Smad2/3 binding regions were calculated for the indicated Smad2/3 binding groups. *E*, frequencies of canonical Smad-binding elements in HNF4α binding regions compared with Smad binding regions in HepG2 cells. A Smad-binding element, M00974.SMAD that was identified as an enriched motif in HepG2-specific Smad2/3 binding regions using CEAS (see text), was selected for calculation. CisGenome was used for mapping of the motif. Presence of the motif for each HNF4α binding region and Smad2/3 binding region was determined using PerlScript.

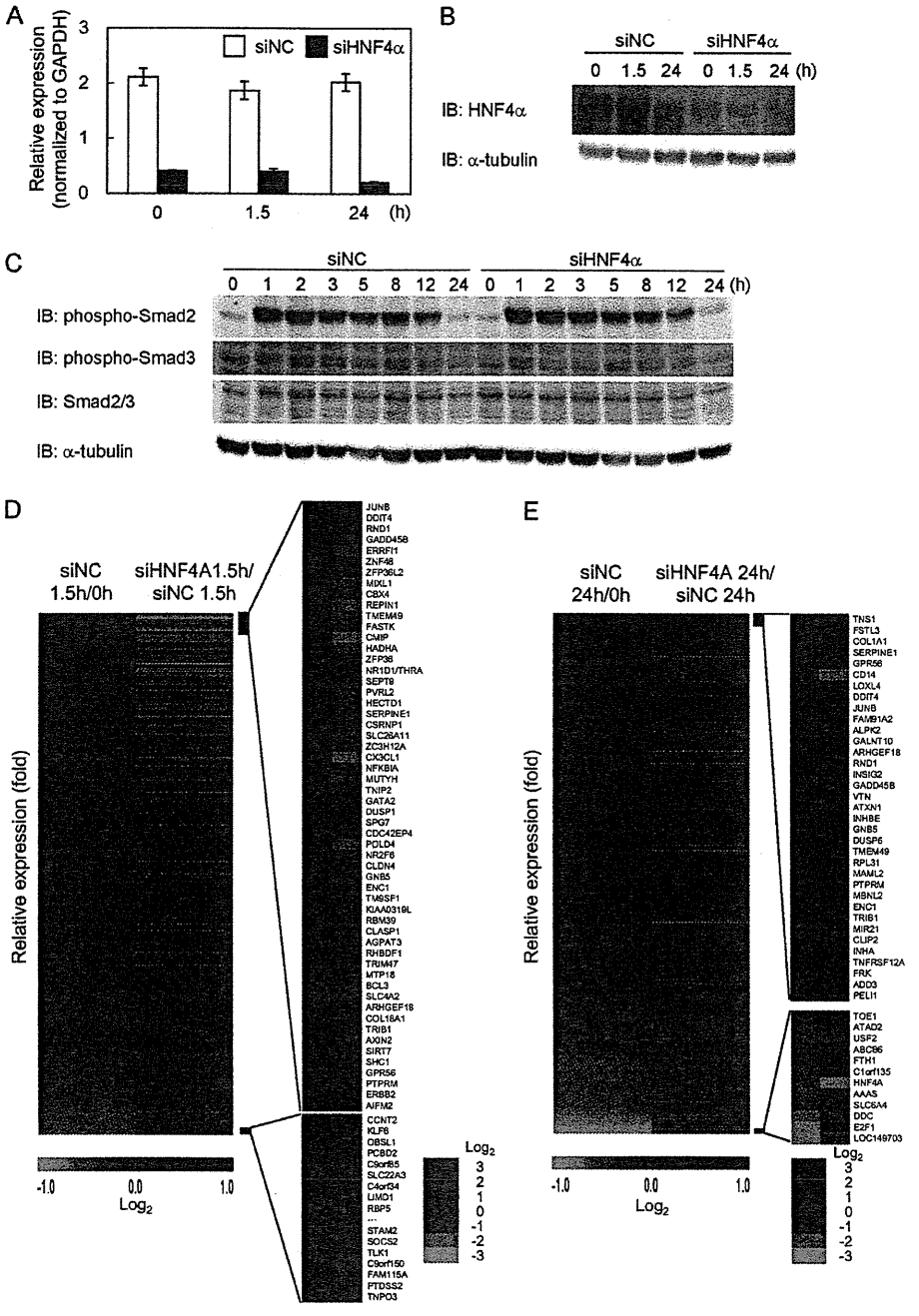

FIGURE 4. **Effect of knockdown of HNF4α on TGF-β-induced gene expression in HepG2 cells.** *A,* confirmation of HNF4α-knocked down samples for microarray analysis. HepG2 cells were transfected with HNF4α siRNA and treated with 120 pM TGF-β for the indicated times and harvested. Expression of HNF4α was determined by RT-qPCR and normalized by glyceraldehyde-3-phosphate dehydrogenase (GAPDH). *siNC,* negative control siRNA. *B,* down-regulation of HNF4α protein expression by siRNA. *C,* phosphorylation levels of Smad2/3 by using HNF4α siRNA. The *top two panels* show phosphorylation of Smad2 and Smad3. The *3rd panel* indicates the expression of total Smad2/3, and the *bottom panel* is a loading control. *IB,* immunoblot. *D,* heat map of the TGF-β-induced expression of target genes of Smad2/3 and HNF4α and effect of HNF4α siRNA. Target genes that have overlapping binding regions of Smad2/3 and HNF4α were sorted by their induction of probe signal values by TGF-β stimulation for 1.5 h and are represented by *color bars* in the *1st column,* using the TM4 microarray software (60). Relative expression of these genes in HNF4α siRNA samples to the control siRNA is shown in the *2nd column.* In addition, a list of genes whose expressions changed more than 1.5-fold is shown in the *right panel* with their expression changes. *E,* heat map of target genes of TGF-β with Smad2/3 binding regions common to HNF4α at 24 h after TGF-β stimulation are shown as in *D.* Genes whose expressions were changed more than 2-fold are shown in the *right panel.*

imity to each other in HepG2 cells, although we could not determine whether HNF4α- and Smad2/3-binding "elements" overlapped within the binding regions because of the limited resolution of ChIP-chip- and ChIP-seq-based assays. We then calculated the frequency of Smad-binding element CAGAC in HNF4α binding regions. 40.4% of the binding regions common to HNF4α and Smad2/3 had Smad-binding elements, compared with 24.3% in the total HNF4α binding regions (Fig. 3*E*).

TABLE 1

TGF-β-induced changes in gene expression in relation to Smad2/3 binding

Expression array data transfected with control siRNA and stimulated with TGF-β were compared with Smad2/3 ChIP-chip data. A total of 8,653 genes that had values of more than 100 at least at one time point for one of their probes (n = 13,720) was used for the analysis. Up-regulated or down-regulated genes were determined compared with 0-h values. The positions of peak signals of Smad binding regions (SBRs) relative to the nearby RefSeq genes were first determined, and regions within 5 kb upstream from the transcription start site and the first intron were selected. *a indicates number of genes analyzed by microarray. *b indicates number of genes which have Smad2/3 binding regions.

		All genes		Genes with SBRs		
		*a	%	*b	%	*b/*a (%)
Total		8653	100.0	1941	100.0	22.4
Increase						
>2-Fold	1.5 h	25	0.3	14	0.7	56.0
	24 h	223	2.6	59	3.0	26.5
>1.5-Fold	1.5 h	273	3.2	89	4.6	32.6
	24 h	837	9.7	250	12.9	29.9
Decrease						
>2-Fold	1.5 h	16	0.2	2	0.1	12.5
	24 h	174	2.0	25	1.3	14.4
>1.5-Fold	1.5 h	217	2.5	47	2.4	21.7
	24 h	877	10.1	160	8.2	18.2

Effect of HNF4α on the Expression of Smad2/3 Target Genes—To elucidate the effect of HNF4α on TGF-β-induced transcriptional regulation, we knocked down HNF4α by using siRNA (Fig. 4, *A* and *B*). The phosphorylation of Smad2 and Smad3 was not affected by the siRNA under the applied condition (Fig. 4*C*). We obtained expression microarray data and calculated the changes in the expression of genes with binding regions shared by Smad2/3 and HNF4α in the presence of TGF-β and siRNA. We first analyzed the data of cells transfected with control siRNA. Twenty four hours after TGF-β stimulation, 4.3 and 21.1% of the genes with Smad2/3 binding regions were regulated (either up- or down-regulated) more than 2- and 1.5-fold, respectively (Table 1). We observed that Smad2/3 binding regions were weakly enriched in the genes up-regulated by TGF-β at 1.5 h (supplemental Fig. S2). Many of the genes with Smad2/3 binding regions were not transcriptionally regulated by TGF-β, and these findings were essentially similar to those in our previous analysis in HaCaT cells (11). We then found that HNF4α siRNA inhibited the expression changes of common target genes of HNF4α and Smad2/3 by TGF-β 1.5 h after stimulation (Fig. 4*D*). This result underscored the general roles of HNF4α in hepatocyte-specific transcriptome regulation by TGF-β. In contrast, the effect of HNF4α silencing was not so obvious in the TGF-β-induced expression changes 24 h after stimulation, compared with the setting after 1.5 h of TGF-β stimulation, although TGF-β-induced expression changes of a subset of genes appeared to be rather enhanced by HNF4α knockdown (Fig. 4*E*). We focused on the changes at 1.5 h, when we obtained Smad2/3 and HNF4α binding data, and we listed target genes of TGF-β and the effect of HNF4α knockdown (Table 2). We identified *MIXL1* as both TGF-β- and HNF4α-regulated gene with no Smad2/3 binding regions in HaCaT cells.

HNF4α Provides a New Mechanism of TGF-β-induced MIXL1 Expression—As shown in Fig. 5*A*, significant binding of Smad2/3 and HNF4α to the *MIXL1* promoter was observed (Fig. 5*A*). We confirmed the binding of these transcription factors by ChIP-qPCR (Fig. 5, *B* and *C*) and changes in the expression of *MIXL1* by HNF4α siRNA by RT-qPCR (Fig. 5*D*). We then determined the sequence of the *MIXL1* promoter bound by Smad2/3 and HNF4α. We first found two possible HNF4α-binding motifs (Fig. 6*A*). Using a promoter reporter assay, we found

TABLE 2

TGF-β-induced genes with Smad2/3 and HNF4α binding at 1.5 h

Target genes of TGF-β in HepG2 cells that were induced more than 2-fold at 1.5 h and that have common binding regions for Smad2/3 and HNF4α were sorted by their expression changes in the presence or absence of HNF4α siRNA. Presence of Smad2/3 binding regions in HaCaT cells is also shown in the 2nd column.

Gene symbol	Smad2/3 binding in HaCaT cells	Relative expression (siNC/siHNF4α)	Induction by TGF-β
		-fold	*-fold*
CMIP	+	0.3	2.1
REPIN1	+	0.3	2.2
MIXL1	−	0.3	2.3
ERRFI1	+	0.4	2.7
FASTK	+	0.5	2.1
ZNF48	−	0.5	2.6
CBX4	−	0.6	2.2
TMEM49	−	0.8	2.1
ZFP36L2	−	0.9	2.6
JUNB	+	1.0	9.8
DDIT4	+	1.1	5.6
GADD45B	+	1.3	4.9
RND1	−	1.4	5.5

that the transcriptional activity of the reporter containing the Smad2/3-HNF4α binding regions was up-regulated by TGF-β, which was significantly repressed by mutations in the HNF4α-binding sequences (Fig. 6*B*). We next searched for canonical Smad-binding elements conserved between mouse and human. We identified three Smad-binding elements between the two HNF4α motifs, and one just upstream of the distal HNF4α motif, termed SBE1 to -4 (Fig. 6*C*). Of them, only a mutation in SBE2 lost TGF-β-induced transcription (Fig. 6*D*). These results suggested that both HNF4α-binding motifs and SBE2 are required for *MIXL1* reporter activity induced by TGF-β.

The transcriptional activity of the reporter was inhibited by HNF4α siRNA, which was observed even without TGF-β, suggesting that preceding binding of HNF4α to its binding motifs as observed in Fig. 5*A* was important both for the basal and TGF-β-induced transcriptional activation of *MIXL1* promoter (Fig. 7*A*). We also investigated the effect of forced HNF4α expression in HaCaT cells to determine whether HNF4α was able to activate the *MIXL1* transcriptional activity in these cells. As shown in Fig. 7*B*, HNF4α induced the transcriptional activity of the *MIXL1* promoter reporter in HaCaT cells. We then examined the effect of a mutant of HNF4α that cannot bind to DNA (HNF4α CR mutant) (32) and found that DNA binding

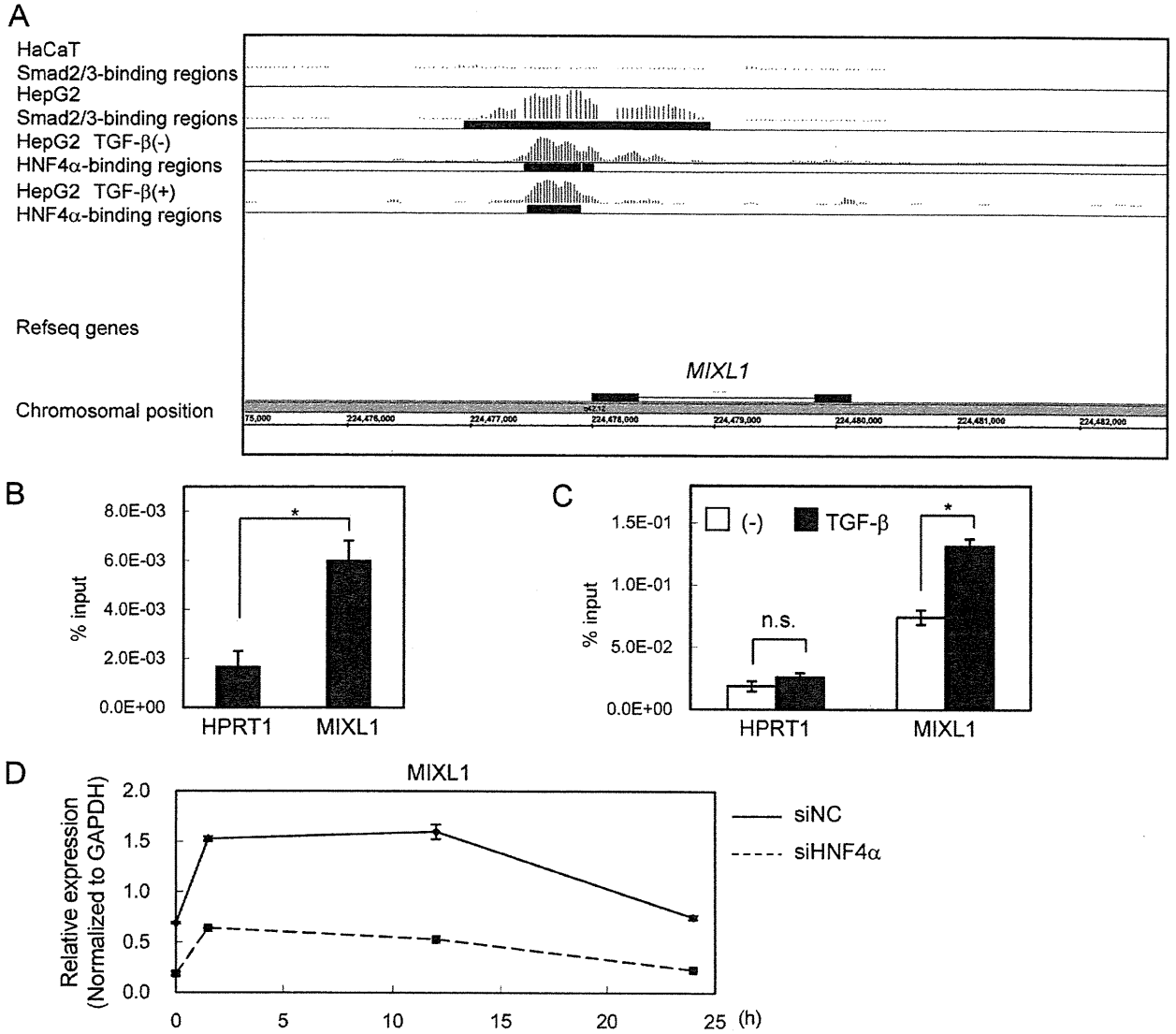

FIGURE 5. **Smad2/3 and HNF4α bindings in the *MIXL1* locus.** *A*, Smad2/3- and HNF4α-enriched regions in the *MIXL1* locus are shown as in Fig. 3*A*. *B*, HepG2 cells were treated with 120 pM TGF-β for 1.5 h, fixed in formaldehyde, and harvested. Smad2/3 binding to the *MIXL1* locus was verified by ChIP-qPCR. *HPRT1* served as a negative control. *C*, HepG2 cells were treated with or without 120 pM TGF-β for 1.5 h, and ChIP-qPCR analysis of the *MIXL1* locus using anti-HNF4α was performed as in *B*. *n.s.*, not significant. *D*, effects of knockdown of HNF4α on TGF-β-induced expression changes of *MIXL1*. HepG2 cells were transfected with control siRNA (*siNC*) or siHNF4α, treated with 3 ng/ml TGF-β for the indicated times, and harvested. HNF4α expression was quantified by RT-qPCR. *, $p < 0.05$; *error bars*, S.D.

activity was required for its TGF-β-induced transcriptional activation (Fig. 7*C*). Finally, the effect of HNF4α siRNA on Smad2/3 binding to the *MIXL1* promoter was determined. HNF4α siRNA inhibited the TGF-β-induced Smad2/3 binding to the *MIXL1* promoter, indicating that the recruitment of Smad2/3 was one of the mechanisms of transcriptional regulation by HNF4α under TGF-β stimulation (Fig. 7*D*).

Taken together, these findings propose that the preceding binding of HNF4α on *MIXL1* promoter enables the recruitment of Smad2/3 to this promoter after TGF-β stimulation and confers TGF-β-mediated HepG2-specific *MIXL1* induction.

DISCUSSION

Recent technological advances, including ChIP-chip and ChIP-seq, provide a functional platform for comprehensive understanding of transcriptional regulation. This study revealed that Smad2/3 binding regions specifically observed in HepG2 cells were enriched in HNF4α binding regions. HNF4α was also expressed in Hep3B cells, and HNF4α-binding motif was identified in Smad2/3 binding regions in Hep3B cells by CEAS analysis (data not shown), which suggests that the functional relation between Smad2/3 and HNF4α is commonly observed in hepatocyte-derived cells. Based on the findings on the HNF4α-Smad interaction (18), physical interaction between HNF4α and Smads is important, at least in part, for TGF-β-induced Smad2/3 binding and transcriptional activation in HepG2 cells. It is also possible that HNF4α has additional indirect interactive functions for TGF-β signaling. Many regulatory mechanisms control the expression of a proper set of genes in various cells and tissues. At the genome level, CpG methylation plays a cen-

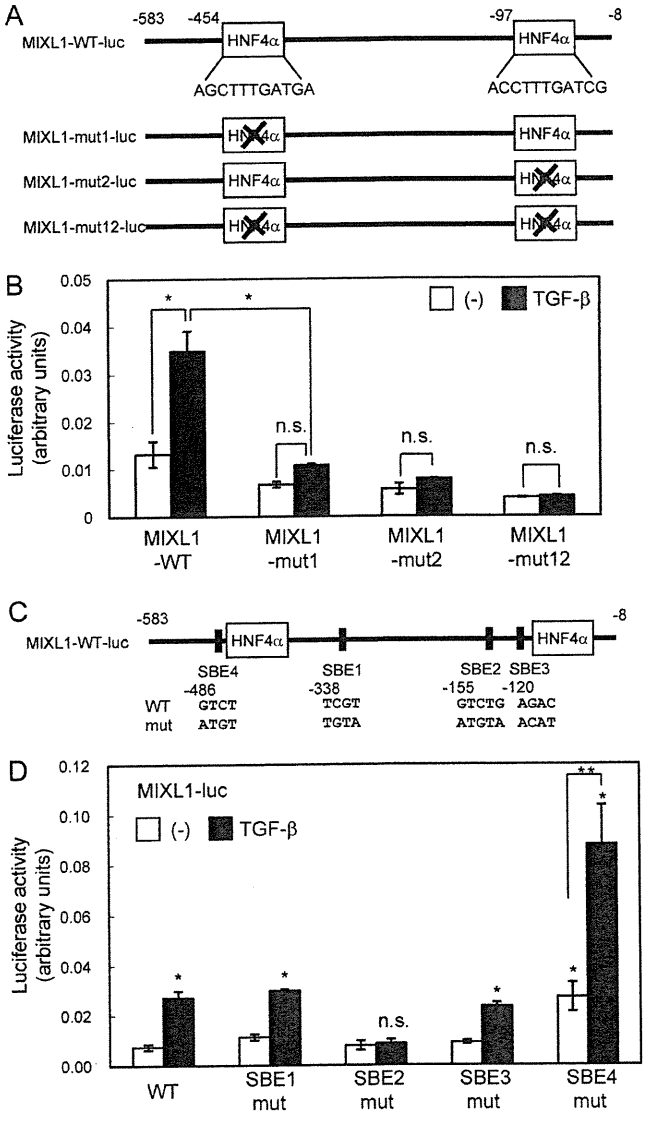

FIGURE 6. **Identification of regulatory elements important for TGF-β-induced transactivation of the *MIXL1* promoter.** *A*, schematic representation of HNF4α-binding motifs in the Smad2/3 and HNF4α binding region of the *MIXL1* promoter. Promoter reporters with mutations in their HNF4α-binding motifs are shown in the *lower panel*. *B*, activation of the *MIXL1* gene promoter by TGF-β and effects of mutations in putative HNF4α-binding motifs. HepG2 cells were transfected with the *MIXL1* promoter and its mutants and treated with TGF-β for 24 h. *C*, conserved Smad-binding elements (*SBEs*) of the *MIXL1* promoter. Four Smad-binding elements that were conserved between mouse and human (SBE 1–4) are shown with their relative positions from the transcription start site. Nucleotide sequences of Smad-binding elements and their mutations used in *D* are also shown. *WT*, wild-type; *mut*, mutant. *D*, effect of mutations in Smad-binding elements on TGF-β-induced transcriptional activity of *MIXL1* promoter. Cells were treated as in *B*, and luciferase activities were determined. *, $p < 0.05$ compared with WT without TGF-β; **, $p < 0.05$ compared with SBE4 mutant, without TGF-β; *n.s.*, not significant compared with WT and SBE2 mutant, without TGF-β; *error bars*, S.D.

tral role to avoid unintended expression of genes that are not suitable for the given tissue (33). Modification of the histone tail is also well known to lead to the formation of either euchromatin or heterochromatin. These modifications of the genome or histones allow transcription factors and cofactors to access the cell- and tissue-specific genomic loci to exert their actions. Modifications of the genome and histones are sometimes induced by *trans* factors during differentiation of the cells and tissues (34, 35). HNF4α physically interacts with the histone acetyltransferase complex and chromatin remodeling complex (29), and it is thus possible that HNF4α induces such epigenomic changes in the liver and indirectly provides Smad2/3 to access to hepatocyte-specific binding regions.

Identification of Smad binding regions downstream of the TGF-β/activin signaling by ChIP-chip analysis has been performed using several cell lines. Recently, Fei *et al.* (36) reported promoter analysis of Smad2 binding regions in mouse embryonic stem cells by ChIP-chip. We and Qin *et al.* (12, 37) analyzed Smad4 binding regions under TGF-β stimulation using HaCaT and ovarian surface epithelial cells, respectively. It has been reported that transcription factor binding regions in the same target gene loci differ among the five vertebrate species (38); it is thus difficult to compare the ChIP-chip or ChIP-seq data obtained from mouse and human. Differences in the ChIP efficiencies of the antibodies also make the comparison of the data difficult (12). Importantly, we used the same antibody and sample preparation procedures for HaCaT cells and HepG2 cells. Our present analysis thus revealed for the first time that Smad binding regions greatly differ among cell lines. Analysis of HaCaT-specific *trans* factors will facilitate our understanding of cell type-specific TGF-β-induced transcription in the future. However, comparison of the number of binding regions in different cell types is still difficult. We found a greater number of Smad2/3 binding regions in HepG2 cells than in HaCaT cells. Because the phosphorylation of Smad3 was weaker and the percent input value of the Smad2/3 ChIP sample was smaller in HepG2 than HaCaT cells, we cannot conclude that HepG2 cells have more Smad2/3 binding regions than HaCaT. It should also be noted that we cannot fully exclude that the antibody recognizes unknown genome-bound molecules in addition to Smad2/3.

Comparison of ChIP-chip and ChIP-seq data of the same transcription factor has been reported (39). In general, ChIP-seq is reported to be more sensitive and specific than ChIP-chip. Oligonucleotide-based array analysis has a potential risk of cross-hybridization and false discovery. Conversely, ChIP-seq also has difficulty in identifying GC-rich sequences (10, 39). We primarily focused on the comparison of our previously reported Smad2/3 binding regions to those of different cell types by the same platform. However, based on the known problems as described above, comparison of the Smad2/3-HNF4α binding regions will be more accurately performed by the ChIP-seq in the future.

Interaction of several transcription factors at the same enhancer positions has been recognized, and the complex is called "enhanceosome." Structure of such complex and their binding DNA motifs have been analyzed in the interferon-β promoter as reviewed by Panne (40). In enhanceosome, each transcription factor physically interacts with others to provide its adequate surface that can bind to the series of their corresponding DNA motifs. Several reports have identified HNF4α binding regions by ChIP-chip and ChIP-seq analyses (29–31, 38, 41–43). Many transcription factors, *e.g.* FOXA2, GABP, HNF1α, HNF4γ, HNF6, cohesin, and CDX2, were identified to

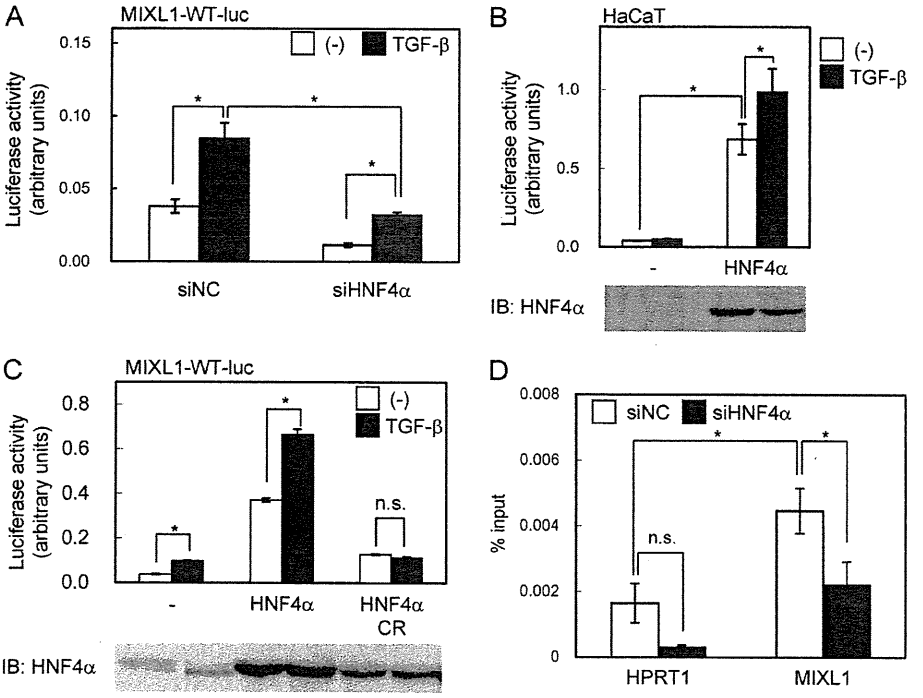

FIGURE 7. **Roles of HNF4α on Smad2/3 binding and transcriptional activity of *MIXL1* promoter.** *A*, effects of HNF4α knockdown on transactivation of the *MIXL1* promoter. HepG2 cells were transfected with siRNAs 1 day before transfection with the reporter constructs. *siNC*, negative control siRNA. *B*, effects of exogenous HNF4α on transactivation of the *MIXL1* promoter. HNF4α was exogenously expressed in HaCaT cells, and transcriptional activity of MIXL1 reporter was determined. The *lower panel* shows the protein expression of HNF4α. *IB*, immunoblot. *C*, HNF4α (variant 2, RefSeq ID: NM_000457) or its C115R (*CR*) mutant, which does not bind to DNA, was overexpressed in HepG2 cells. The *lower panel* shows the protein expression of HNF4α and its mutant. *D*, effect of HNF4α siRNA on Smad2/3 binding to the *MIXL1* locus. HepG2 cells were transfected with siRNAs 24 h before TGF-β stimulation. Cells were fixed 1.5 h after treatment, and ChIP-qPCR was performed as in Fig. 1*B*. *Error bars*, S.D.; *, $p < 0.05$; *n.s.*, not significant.

co-localize with HNF4α through these analyses. Other reports also revealed interaction of FOXO1 or retinoic acid receptor/retinoid X receptor with HNF4α on specific promoters (44, 45). These findings clearly revealed steady-state binding regions of HNF4α on the genome and suggested that transcription factors that co-localize or interact with HNF4α may form enhanceosome with HNF4α. Changes in the HNF4α binding regions were found during differentiation of an intestinal epithelial cell line CaCo2 (43); however, to our knowledge, the effect of single extracellular stimulation on genome-wide HNF4α binding regions has not yet been elucidated. Our present analysis provides the data of HNF4α binding regions following TGF-β stimulation, which were compared with the Smad2/3 binding regions in HaCaT cells that lack the expression of HNF4α. We have found that large proportions of HNF4α binding regions in HepG2 cells were unchanged by TGF-β stimulation. However, some changes in HNF4α binding regions were observed with regard to their positions and their strength, suggesting that TGF-β might regulate a subset of HNF4α binding regions. de Boussac *et al.* (46) reported that hepatocyte growth factor inhibited HNF4α binding to the *ABCC6* promoter, which together suggest the importance of changes in the HNF4α binding positions by external stimuli. We also found that the effect of HNF4α on the TGF-β-induced gene expression after 24 h of TGF-β stimulation was different from that after 1.5 h of TGF-β stimulation. Studies on the changes in the genome-wide HNF4α and Smad2/3 binding after TGF-β stimulation at several time points and ChIP-seq analysis of HNF4α with other interactive factors in relation to their binding DNA sequences will reveal new mechanisms of the regulation of HNF4α-induced transcription in the context of the enhanceosome.

MIXL1 is an ortholog of *Xenopus* Mix.1, a transcription factor rapidly induced by activin during the early stage of *Xenopus* development (47). There are six known homologs that have been identified in *Xenopus* to engage in the formation of mesoderm and endoderm (48, 49). However, only one ortholog of Mix.1 is known in human and mouse (50). MIXL1 is required for the development of the chordamesoderm, heart, and gut in mouse (51). Forced expression of MIXL1 in embryonic stem cells resulted in the differentiation of the cells to endoderm (52). TGF-β is reported to induce *Mix.2* promoter activity by formation of a Smad2/Smad4/FAST-1 (FoxH1) complex (53). In mouse, Smads and FAST-1 interact to up-regulate the transcriptional activity of the *MIXL1* promoter (54, 55). However, FAST-1 is not expressed in HepG2 cells (56). Our finding of TGF-β-induced *MIXL1* expression in HepG2 cells suggests a previously unrecognized regulatory mechanism of its expression by HNF4α in the absence of FAST-1. During development, HNF4α is expressed in the visceral endoderm during the gastrulation stage and plays a role in the differentiation of the embryonic mesoderm (57). MIXL1 is also expressed in the visceral endoderm and induces migration of the embryonic endoderm. HNF4α-null mice embryo showed impaired development of mature visceral endoderm, indicating that HNF4α acts upstream of MIXL1, at least in the visceral endoderm. Notably, both HNF4α and MIXL1 positively reg-

ulate the E-cadherin expression (52, 58), and the HNF4α expression was repressed in a model of progression of hepatocellular carcinoma (59). Functional analysis of MIXL1 in liver fibrosis and hepatocellular carcinoma in relation to TGF-β signaling might reveal the roles of MIXL1 in the adult liver in the future.

Acknowledgments—We thank Keiko Yuki, Hiroko Meguro, and Kaori Shiina for technical assistance.

REFERENCES

1. Ikushima, H., and Miyazono, K. (2010) *Nat. Rev. Cancer* **10,** 415–424
2. Heldin, C. H., Miyazono, K., and ten Dijke, P. (1997) *Nature* **390,** 465–471
3. Feng, X. H., and Derynck, R. (2005) *Annu. Rev. Cell Dev. Biol.* **21,** 659–693
4. Miyazono, K., Kamiya, Y., and Morikawa, M. (2010) *J. Biochem.* **147,** 35–51
5. Shi, Y., Wang, Y. F., Jayaraman, L., Yang, H., Massagué, J., and Pavletich, N. P. (1998) *Cell* **94,** 585–594
6. Zawel, L., Dai, J. L., Buckhaults, P., Zhou, S., Kinzler, K. W., Vogelstein, B., and Kern, S. E. (1998) *Mol. Cell* **1,** 611–617
7. Ikushima, H., and Miyazono, K. (2010) *Cancer Sci.* **101,** 306–312
8. Gomis, R. R., Alarcón, C., He, W., Wang, Q., Seoane, J., Lash, A., and Massagué, J. (2006) *Proc. Natl. Acad. Sci. U.S.A.* **103,** 12747–12752
9. Eeckhoute, J., Lupien, M., and Brown, M. (2009) *Methods Mol. Biol.* **556,** 155–164
10. Park, P. J. (2009) *Nat. Rev. Genet.* **10,** 669–680
11. Koinuma, D., Tsutsumi, S., Kamimura, N., Taniguchi, H., Miyazawa, K., Sunamura, M., Imamura, T., Miyazono, K., and Aburatani, H. (2009) *Mol. Cell. Biol.* **29,** 172–186
12. Koinuma, D., Tsutsumi, S., Kamimura, N., Imamura, T., Aburatani, H., and Miyazono, K. (2009) *Cancer Sci.* **100,** 2133–2142
13. Sladek, F. M., Zhong, W. M., Lai, E., and Darnell, J. E., Jr. (1990) *Genes Dev.* **4,** 2353–2365
14. Si-Tayeb, K., Lemaigre, F. P., and Duncan, S. A. (2010) *Dev. Cell* **18,** 175–189
15. Jiang, G., Nepomuceno, L., Hopkins, K., and Sladek, F. M. (1995) *Mol. Cell. Biol.* **15,** 5131–5143
16. Lucas Sd, S., López-Alcorocho, J. M., Bartolomé, J., and Carreño, V. (2004) *Biochem. Biophys. Res. Commun.* **321,** 688–694
17. Ishikawa, F., Nose, K., and Shibanuma, M. (2008) *Exp. Cell Res.* **314,** 2131–2140
18. Kardassis, D., Pardali, K., and Zannis, V. I. (2000) *J. Biol. Chem.* **275,** 41405–41414
19. Chou, W. C., Prokova, V., Shiraishi, K., Valcourt, U., Moustakas, A., Hadzopoulou-Cladaras, M., Zannis, V. I., and Kardassis, D. (2003) *Mol. Biol. Cell* **14,** 1279–1294
20. Mizutani, A., Saitoh, M., Imamura, T., Miyazawa, K., and Miyazono, K. (2010) *J. Biochem.* **148,** 733–741
21. Wendt, K. S., Yoshida, K., Itoh, T., Bando, M., Koch, B., Schirghuber, E., Tsutsumi, S., Nagae, G., Ishihara, K., Mishiro, T., Yahata, K., Imamoto, F., Aburatani, H., Nakao, M., Imamoto, N., Maeshima, K., Shirahige, K., and Peters, J. M. (2008) *Nature* **451,** 796–801
22. Kaneshiro, K., Tsutsumi, S., Tsuji, S., Shirahige, K., and Aburatani, H. (2007) *Genomics* **89,** 178–188
23. Johnson, W. E., Li, W., Meyer, C. A., Gottardo, R., Carroll, J. S., Brown, M., and Liu, X. S. (2006) *Proc. Natl. Acad. Sci. U.S.A.* **103,** 12457–12462
24. Ji, H., Jiang, H., Ma, W., Johnson, D. S., Myers, R. M., and Wong, W. H. (2008) *Nat. Biotechnol.* **26,** 1293–1300
25. Ji, X., Li, W., Song, J., Wei, L., and Liu, X. S. (2006) *Nucleic Acids Res.* **34,** W551–W554
26. Nagano, Y., Koinuma, D., Miyazawa, K., and Miyazono, K. (2010) *J. Biochem.* **147,** 545–554
27. Huang da, W., Sherman, B. T., and Lempicki, R. A. (2009) *Nat. Protoc.* **4,** 44–57
28. Portales-Casamar, E., Thongjuea, S., Kwon, A. T., Arenillas, D., Zhao, X., Valen, E., Yusuf, D., Lenhard, B., Wasserman, W. W., and Sandelin, A. (2010) *Nucleic Acids Res.* **38,** D105–D110
29. Daigo, K., Kawamura, T., Ohta, Y., Ohashi, R., Katayose, S., Tanaka, T., Aburatani, H., Naito, M., Kodama, T., Ihara, S., and Hamakubo, T. (2011) *J. Biol. Chem.* **286,** 674–686
30. Wallerman, O., Motallebipour, M., Enroth, S., Patra, K., Bysani, M. S., Komorowski, J., and Wadelius, C. (2009) *Nucleic Acids Res.* **37,** 7498–7508
31. Schmidt, D., Schwalie, P. C., Ross-Innes, C. S., Hurtado, A., Brown, G. D., Carroll, J. S., Flicek, P., and Odom, D. T. (2010) *Genome Res.* **20,** 578–588
32. Taylor, D. G., Haubenwallner, S., and Leff, T. (1996) *Nucleic Acids Res.* **24,** 2930–2935
33. Bernstein, B. E., Meissner, A., and Lander, E. S. (2007) *Cell* **128,** 669–681
34. Kim, M. S., Kondo, T., Takada, I., Youn, M. Y., Yamamoto, Y., Takahashi, S., Matsumoto, T., Fujiyama, S., Shirode, Y., Yamaoka, I., Kitagawa, H., Takeyama, K., Shibuya, H., Ohtake, F., and Kato, S. (2009) *Nature* **461,** 1007–1012
35. Lan, F., Nottke, A. C., and Shi, Y. (2008) *Curr. Opin. Cell Biol.* **20,** 316–325
36. Fei, T., Zhu, S., Xia, K., Zhang, J., Li, Z., Han, J. D., and Chen, Y. G. (2010) *Cell Res.* **20,** 1306–1318
37. Qin, H., Chan, M. W., Liyanarachchi, S., Balch, C., Potter, D., Souriraj, I. J., Cheng, A. S., Agosto-Perez, F. J., Nikonova, E. V., Yan, P. S., Lin, H. J., Nephew, K. P., Saltz, J. H., Showe, L. C., Huang, T. H., and Davuluri, R. V. (2009) *BMC Syst. Biol.* **3,** 73
38. Schmidt, D., Wilson, M. D., Ballester, B., Schwalie, P. C., Brown, G. D., Marshall, A., Kutter, C., Watt, S., Martinez-Jimenez, C. P., Mackay, S., Talianidis, I., Flicek, P., and Odom, D. T. (2010) *Science* **328,** 1036–1040
39. Ho, J. W., Bishop, E., Karchenko, P. V., Nègre, N., White, K. P., and Park, P. J. (2011) *BMC Genomics* **12,** 134
40. Panne, D. (2008) *Curr. Opin. Struct. Biol.* **18,** 236–242
41. Boyd, M., Bressendorff, S., Møller, J., Olsen, J., and Troelsen, J. T. (2009) *BMC Gastroenterol.* **9,** 68
42. Odom, D. T., Zizlsperger, N., Gordon, D. B., Bell, G. W., Rinaldi, N. J., Murray, H. L., Volkert, T. L., Schreiber, J., Rolfe, P. A., Gifford, D. K., Fraenkel, E., Bell, G. I., and Young, R. A. (2004) *Science* **303,** 1378–1381
43. Verzi, M. P., Shin, H., He, H. H., Sulahian, R., Meyer, C. A., Montgomery, R. K., Fleet, J. C., Brown, M., Liu, X. S., and Shivdasani, R. A. (2010) *Dev. Cell* **19,** 713–726
44. Ganjam, G. K., Dimova, E. Y., Unterman, T. G., and Kietzmann, T. (2009) *J. Biol. Chem.* **284,** 30783–30797
45. Mosialou, I., Zannis, V. I., and Kardassis, D. (2010) *J. Biol. Chem.* **285,** 30719–30730
46. de Boussac, H., Ratajewski, M., Sachrajda, I., Köblös, G., Tordai, A., Pulaski, L., Buday, L., Váradi, A., and Arányi, T. (2010) *J. Biol. Chem.* **285,** 22800–22808
47. Rosa, F. M. (1989) *Cell* **57,** 965–974
48. Ecochard, V., Cayrol, C., Rey, S., Foulquier, F., Caillol, D., Lemaire, P., and Duprat, A. M. (1998) *Development* **125,** 2577–2585
49. Vize, P. D. (1996) *Dev. Biol.* **177,** 226–231
50. Robb, L., Hartley, L., Begley, C. G., Brodnicki, T. C., Copeland, N. G., Gilbert, D. J., Jenkins, N. A., and Elefanty, A. G. (2000) *Dev. Dyn.* **219,** 497–504
51. Hart, A. H., Hartley, L., Sourris, K., Stadler, E. S., Li, R., Stanley, E. G., Tam, P. P., Elefanty, A. G., and Robb, L. (2002) *Development* **129,** 3597–3608
52. Lim, S. M., Pereira, L., Wong, M. S., Hirst, C. E., Van Vranken, B. E., Pick, M., Trounson, A., Elefanty, A. G., and Stanley, E. G. (2009) *Stem Cells* **27,** 363–374
53. Watanabe, M., and Whitman, M. (1999) *Development* **126,** 5621–5634
54. Hart, A. H., Willson, T. A., Wong, M., Parker, K., and Robb, L. (2005) *Biochem. Biophys. Res. Commun.* **333,** 1361–1369
55. Izzi, L., Silvestri, C., von Both, I., Labbé, E., Zakin, L., Wrana, J. L., and Attisano, L. (2007) *EMBO J.* **26,** 3132–3143
56. Hayashi, H., Abdollah, S., Qiu, Y., Cai, J., Xu, Y. Y., Grinnell, B. W., Richa-

rdson, M. A., Topper, J. N., Gimbrone, M. A., Jr., Wrana, J. L., and Falb, D. (1997) *Cell* **89,** 1165–1173
57. Chen, W. S., Manova, K., Weinstein, D. C., Duncan, S. A., Plump, A. S., Prezioso, V. R., Bachvarova, R. F., and Darnell, J. E., Jr. (1994) *Genes Dev.* **8,** 2466–2477
58. Späth, G. F., and Weiss, M. C. (1998) *J. Cell Biol.* **140,** 935–946
59. Lazarevich, N. L., Cheremnova, O. A., Varga, E. V., Ovchinnikov, D. A., Kudrjavtseva, E. I., Morozova, O. V., Fleishman, D. I., Engelhardt, N. V., and Duncan, S. A. (2004) *Hepatology* **39,** 1038–1047
60. Saeed, A. I., Bhagabati, N. K., Braisted, J. C., Liang, W., Sharov, V., Howe, E. A., Li, J., Thiagarajan, M., White, J. A., and Quackenbush, J. (2006) *Methods Enzymol.* **411,** 134–193

8712–8727 Nucleic Acids Research, 2011, Vol. 39, No. 20
doi:10.1093/nar/gkr572

Published online 15 July 2011

ChIP-seq reveals cell type-specific binding patterns of BMP-specific Smads and a novel binding motif

Masato Morikawa[1], Daizo Koinuma[1], Shuichi Tsutsumi[2], Eleftheria Vasilaki[3], Yasuharu Kanki[4], Carl-Henrik Heldin[3], Hiroyuki Aburatani[2] and Kohei Miyazono[1,3,*]

[1]Department of Molecular Pathology, Graduate School of Medicine, University of Tokyo, Bunkyo-ku, Tokyo 113-0033, [2]Genome Science Division, Research Center for Advanced Science and Technology, University of Tokyo, Meguro-ku, Tokyo 153-8904, Japan, [3]Ludwig Institute for Cancer Research, Box 595 Biomedical Center, SE-751 24 Uppsala, Sweden and [4]Laboratory for Systems Biology and Medicine, Research Center for Advanced Science and Technology, University of Tokyo, Meguro-ku, Tokyo 153-8904, Japan

Received May 13, 2011; Revised and Accepted June 24, 2011

ABSTRACT

Dysregulated bone morphogenetic protein (BMP) signaling in endothelial cells (ECs) and pulmonary arterial smooth muscle cells (PASMCs) are implicated in human genetic disorders. Here, we generated genome-wide maps of Smad1/5 binding sites in ECs and PASMCs. Smad1/5 preferentially bound to the region outside the promoter of known genes, and the binding was associated with target gene upregulation. Cell-selective Smad1/5 binding patterns appear to be determined mostly by cell-specific differences in baseline chromatin accessibility patterns. We identified, for the first time, a Smad1/5 binding motif in mammals, and termed GC-rich Smad binding element (GC-SBE). Several sequences in the identified GC-SBE motif had relatively weak affinity for Smad binding, and were enriched in cell type-specific Smad1/5 binding regions. We also found that both GC-SBE and the canonical SBE affect binding affinity for the Smad complex. Furthermore, we characterized EC-specific Smad1/5 target genes and found that several Notch signaling pathway-related genes were induced by BMP in ECs. Among them, a Notch ligand, JAG1 was regulated directly by Smad1/5, transactivating Notch signaling in the neighboring cells. These results provide insights into the molecular mechanism of BMP signaling and the pathogenesis of vascular lesions of certain genetic disorders, including hereditary hemorrhagic telangiectasia.

INTRODUCTION

Bone morphogenetic proteins (BMPs) are members of the transforming growth factor-β (TGF-β) family, which regulate a variety of cellular processes including differentiation, proliferation, migration and cell death in a cell type-specific and context-dependent manner (1). Perturbations of BMP signaling pathways have been implicated in a diverse set of developmental disorders, tumorigenesis and diseases including ectopic ossification and cardiovascular diseases. Mutations in *ENG*, *ACVRL1* or *SMAD4* genes have been shown to cause hereditary hemorrhagic telangiectasia (HHT) (2–4), which is a multisystemic vascular disorder characterized by epistaxis, telangiectases and arteriovenous malformation (AVM). The *ACVRL1* gene encodes an endothelial-specific type I receptor for TGF-β members, ALK-1, whose signals are transmitted through BMP-specific receptor-regulated Smads (BR-Smads; Smad1/5/8) (5). Recent work has indicated that haploinsufficiency of ALK-1 causes HHT (6). The *ENG* gene encodes Endoglin, which is an endothelial expressed co-receptor and modulates ALK-1 signaling (7). The *SMAD4* gene encodes a common mediator Smad (co-Smad), which makes a heterotrimeric complex with BR-Smads and regulate transcription of specific target genes (8). Therefore, dysregulated BMP signaling through ALK-1 in endothelial cells (ECs) is implicated in the pathogenesis of HHT. Interestingly, BMP signaling activated by BMP type I receptors, other than ALK-1 in ECs, are not able to compensate for the loss of function of ALK-1. On the other hand, aberrant BMP signaling through BMP type II receptor (encoded by *BMPR2*), especially in pulmonary arterial smooth muscle cells (PASMCs), are implicated in the pathogenesis of pulmonary arterial hypertension (PAH) (9,10). Therefore, readout of BMP signaling depends on the strength of BMP signaling, types I and II receptors and co-receptors, and cell types.

A binding sequence for BR-Smad was originally identified in *Drosophila*. Kim and colleagues (11) indicated that GCCGnCGC is a consensus binding sequence for Mad (*Drosophila* Smad1). In mammals, similar GC-rich

*To whom correspondence should be addressed. Tel: +81 3 5841 3356; Fax: +81 3 5841 3354; Email: miyazono@m.u-tokyo.ac.jp

sequences, e.g. GCCG or GGCGCC, have been evaluated in the promoter regions of well-known BMP target genes (12,13). Recombinant protein of the DNA binding domain of mouse Smad1 (Smad1 MH1) has been shown to bind to the GGCGCC sequence *in vitro* (14). This GGCGCC sequence is widely accepted as a binding sequence for BR-Smads, while a binding motif for BR-Smad has not been clearly defined in mammals.

Recent advances in microarray and sequencing technologies have made it possible to analyze global gene expression profiles and genome-wide maps of protein binding sites or epigenetic marks (15). Two groups have reported genome-wide analyses of BR-Smads in mouse ES cells (mESCs) using chromatin immunoprecipitation (ChIP) coupled with promoter array (ChIP-chip) and ChIP followed by sequencing (ChIP-seq) analyses (16,17). Through profiling of the global binding sites of 13 transcription factors and 2 transcription regulators in mESCs, Chen and colleagues (16) hypothesized that Smad1 makes an enhancer complex with Sox2-Oct4 (also known as Pou5F1), which defines ES-specific binding patterns of Smads. However, it has not been clarified whether a transcription factor complex, or an enhancer complex, determines the cell type-specific binding patterns of Smads in other cell types.

Here, we performed ChIP-seq to map Smad1/5 occupancy at high resolution in two different primary human cells treated with several BMP isoforms; human umbilical vein endothelial cells (HUVECs) with BMP-9 or BMP-6 and PASMCs with BMP-4. Smad1/5 preferentially bound to the region outside the promoter of known genes, and their binding was associated with upregulation of target genes. In HUVECs, Smad1/5 binding regions overlapped with reported enhancer regions. Comparison of HUVECs and PASMCs revealed that about 20% of the binding regions were overlapped. In contrast, most of the Smad1/5 binding sites in HUVECs treated with BMP-6 overlapped with those with BMP-9, especially in the regions with higher affinity for Smads. Cell-selective Smad1/5 binding patterns appear to be determined mostly by cell-specific differences in baseline chromatin accessibility patterns. In addition, a Smad1/5 binding motif was identified and termed a GC-rich Smad Binding Element (GC-SBE). Interestingly, GGAGCC sequence was enriched in the HUVEC- or PASMC-specific Smad1/5 binding regions compared with the GGCGCC sequence. We revealed that mutations of GC-SBE affected binding of Smad complex in a cell type-specific manner. Furthermore, we characterized EC-specific Smad1/5 target genes and found that several Notch signaling pathway-related genes were induced in ECs. Among them, a Notch ligand, JAG1 was regulated directly by Smad1/5, transactivating Notch signaling in the neighboring cells. These results provide insights into the molecular mechanism of BMP signaling and the pathogenesis of vascular lesions of HHT.

MATERIALS AND METHODS

Cell culture

HEK293T, HepG2 and HeLa cells were obtained from the American Type Culture Collection (ATCC). HUVECs and PASMCs were obtained from Lonza. HMEC-1, an immortalized human dermal microvascular EC line, was obtained from Dr T. Lawley (Emory University, Atlanta, GA, USA). 293T, HepG2 and HeLa cells were maintained in Dulbecco's modified Eagle's medium (Gibco), supplemented with 10% (v/v) fetal bovine serum (FBS) (HyClone) and 1% penicillin–streptomycin (Gibco). HUVECs and HMEC-1 were cultured in EGM-2 medium (Lonza). PASMCs were cultured in SmGM-2 (Lonza).

Reagents and antibodies

Recombinant human BMP-4, BMP-6 and BMP-9 were purchased from R&D Systems. TNF-α was from PeproTech. Cycloheximide (CHX) was purchased from Sigma-Aldrich.

The following antibodies were used: anti-Flag M2 (Sigma-Aldrich), anti-α-tubulin (AC-15; Sigma-Aldrich), anti-HDAC-1 (2E10; Upstate Millipore), anti-Smad1 (Bio Matrix Research, Chiba, Japan), which recognizes both Smad1 and Smad5 for ChIP procedure, anti-Smad1/5/8 (N-18; Santa Cruz Biotechnology) for western blotting, anti-phospho-Smad1/5 (Cell Signaling Technology), anti-phospho-Smad1/5/8 (Cell Signaling) and anti-JAG1 (H-114; Santa Cruz).

ChIP

Chromatin isolation, sonication and immunoprecipitation (IP) using anti-Smad1/5 antibody were performed essentially as described (18).

ChIP-sequencing (ChIP-seq) and data analysis

High-throughput sequencing of the ChIP fragments was performed using Illumina Genome Analyzer (Illumina) following the manufacturer's protocols. One flow cell lane was used for sequencing of each pooled sample. Unfiltered 36 bp sequence reads were aligned against the human reference genome (NCBI Build 36, hg18) using ELAND (Illumina). Peaks were called using CisGenome v1.2 (19) by two-sample analysis, where input genomic DNA was used as a negative control (Supplementary Table S1). Assigning a binding site to the nearest gene within 100 kb from a peak was performed using CisGenome.

A set of random genomic control regions for 3750 Smad1/5 binding regions was generated by randomly picking up the same number of 301 bp chromosome-matched sequences. In order to calculate the frequency of transcription factor binding site (TFBS)-positive sequences, MATCH score of position-specific scoring matrix (PSSM) for each transcription factor was computed. The highest MATCH score (HMS) was assigned to each sequence, and the number of sequences with HMS greater than or equal to a threshold was counted. For obtaining background data against those of 3750 Smad1/5 binding regions, the chromosome-matched sequences were generated randomly for 1000 times. The distribution of HMSs in 1000 sets of 3750 sequences was used as background control for each PSSM. The threshold was set to the mode of the distribution of HMSs. PSSMs

were obtained from JASPAR database (20). A set of non-overlapping matched genomic control sequences was generated by CisGenome. The frequency of TFBSs in these sequences (motif counts per set of sequences) was computed with the likelihood ratio ≥500 (default value of CisGenome) or 200 (for shorter motifs such as MEME4). Fifty sets of matched control sequences were used as background data. Mapping of TFBSs to the specific genomic regions were calculated by the CisGenome.

The sequences of Smad1/5 binding sites were input to the MEME (21) with several options: mod = oops, nmotifs = 5, minw = 6, maxw = 8, revcomp and other settings default. The logo plots were generated using the seqLogo package in R (http://bioconductor.org/packages/2.6/bioc/html/seqLogo.html). Enriched binding motifs were also obtained from the Cis-regulatory Element Annotation System (CEAS) website as described (http://ceas.cbi.pku.edu.cn/index.html) (22,23). Overrepresented gene ontology (GO) categories for genes associated with Smad1/5 binding regions were determined using the Database for Annotation, Visualization and Integrated Discovery (DAVID v6.7; http://david.abcc.ncifcrf.gov) (24).

ChIP and quantitative-PCR

The real-time PCR was conducted as described (23). Primer sequences are given in Supplementary Table S2 in the Supplementary Data. The amount of immunoprecipitated DNA was calculated relative to the input.

RNA isolation, quantitative real-time reverse transcription–PCR and conventional RT–PCR

Extraction of total RNA, qRT–PCR and conventional RT–PCR were performed as described (23). Primer sequences are given in Supplementary Table S2.

Gene expression profiling

HUVECs and PASMCs were serum starved overnight and treated with or without BMP-9 (1 ng/ml), BMP-6 or BMP-4 (50 ng/ml) treatment for 2 or 24 h. Gene expression profiling was performed with a GeneChip Human Genome U133 Plus 2.0 Array (Affymetrix) as described (18). The 8544 and 8067 genes, whose signal intensity exceeded 100 at any time point were considered to be expressed and functional in HUVECs and PASMCs, respectively. The heatmaps were produced using the heatmap.2 function from the gplots library in R (http://cran.r-project.org/web/packages/gplots/).

Histone modification data

Genome-wide histone modification map for monomethylation of histone H3 lysine 4 (H3K4me1), trimethylation of histone H3 lysine 4 (H3K4me3) and acetylation of histone H3 lysine 27 (H3K27ac) of HUVECs were produced and released from the ENCODE Project (25) and were downloaded from UCSC (http://hgdownload.cse.ucsc.edu/goldenPath/hg18/encodeDCC/wgEncodeBroadChipSeq/).

Plasmid construction

FLAG-tagged Smad constructs were previously described (18). Each fragment of Smad1/5 binding regions was amplified from human genomic DNA by PCR, cloned into a modified pGL4.10 reporter plasmid (Promega) driven by minimal adenoviral major late promoter (MLP) (12). A point mutation was introduced by site-directed mutagenesis using PCR with specific primers. A reporter construct with six multimerized CTGGAGCC sequence (pGL4-6xGC-SBE-Luc) was constructed as follows. A fragment with one copy of the CTGGAGCC sequence was cloned into the pcDNA3.1 vector (Invitrogen). The sequences of the oligonucleotides were 5′-AGATCTTCGAACAGCTC TGGAGCCAGATGGCCTGGATCC-3′ (sense) and 5′-G GATCCAGGCCATCTGGCTCCAGAGCTGTTCGAA GATCT-3′ (antisense). This fragment was multimerized in tandem, and the fragment containing six tandem copies was subcloned into the modified pGL4-MLP plasmid. Six multimerized dimeric CBF1/Suppressor of Hairless/Lag1 (CSL) binding sites with Epstein-Barr virus (EBV) TP1 promoter sequence of the pGA981-6 (26) was transferred into pGL4.10 reporter plasmid (pGL4-12xCSL-Luc) and used for Notch reporter assay. A plasmid encoding GST-hSmad1-MH1 was constructed by PCR amplification of the MH1 domain of human Smad1 (1–143 amino acid). The fragment was subcloned into pGEX-6P-1 vector (GE Healthcare, Chalfont St Giles, UK). All constructs were DNA sequence verified.

Protein production and purification

The bacterially expressed GST fusion proteins containing residues for human $Smad1_{1-143}$ (GST-hSmad1-MH1) were purified with Glutathione Sepharose 4B beads (GE Healthcare) followed by cleavage with PreScission Protease (GE Healthcare) at 4°C overnight according to the recommendations of the manufacturer. The concentration of the protein was measured by BCA Protein Assay Kit (Pierce).

Electrophoretic mobility shift assays

Electrophoretic mobility shift assays (EMSA) was conducted essentially as described previously (14) and detected with LightShift Chemiluminescent EMSA kit (Pierce). The sequences of the DNA oligos are provided in Supplementary Table S2.

Lentiviral infection and luciferase assays

Since transfection efficacy is very low in HUVECs and it is rather toxic, we adapted lentiviral expression system. pGL4 constructs were subcloned between EcoRI and XhoI sites of the lentiviral vector construct CS-CDF-CG-PRE. Recombinant lentiviral vectors were generated as reported previously (23).

Stably expressing cells were stimulated with indicated doses of BMP-9 or BMP-6, and then they were harvested and assayed for luciferase activity at 12 h after stimulation. Luciferase activities of the cell lysates were determined using the Dual-luciferase Reporter Assay System (Promega).

Transient transfection and dual-luciferase assays

Transient transfection was carried out using FuGENE 6 (Roche) for HEK293T cells, Lipofectamine 2000 (Invitrogen) for HepG2 cells and Lipofectamine LTX (Invitrogen) for HMEC-1 cells and PASMCs according to the recommendations of the manufacturer.

Cells were transiently transfected with 1 μg of the luciferase reporter constructs along with 0.05 μg of Renilla luciferase reporter vector pGL4.74[hRluc/TK] (Promega) as an internal control. For HMEC-1 and PASMCs, the medium was changed at 3 h after transfection. Cells were stimulated with 1 ng/ml BMP-9 (HMEC-1), 50 ng/ml BMP-6 (HepG2) or 30 ng/ml BMP-4 (PASMCs) at 24 h after transfection, and then they were harvested and assayed for luciferase activity at 16 h after stimulation.

RNA interference

Duplexes of small interfering RNA (siRNA) against human Smad4 (D-003902-05) were synthesized by Dharmacon (Thermo Fisher Scientific), and were transfected using Lipofectamine RNAiMAX (Invitrogen) according to the recommendations of the manufacturer. The final concentration of siRNA in the culture media was 10 nM. At 24 h after transfection, cells were serum starved overnight, treated with or without BMP-9 for 2 or 24 h and subjected to qRT–PCR.

Western blotting

Western blotting was performed essentially as described (18). Cytoplasmic and nuclear fractions were isolated using NE-PER Nuclear and Cytoplasmic Extraction Reagents (Pierce) according to the recommendations of the manufacturer.

Immunofluorescence microscopy

HUVECs were treated with 1 ng/ml BMP-9 for 24 h, fixed in 10% formalin for 20 min and incubated overnight at 4°C with primary antibodies (JAG1, 1:100 dilution) diluted in Blocking One solution (Nacalai Tesque, Kyoto, Japan). The cells were washed with PBST (PBS with 0.1% Triton X-100), and then incubated with secondary antibodies (Alexa Fluor 488 goat anti-rabbit IgG, Invitrogen, 1:500 dilution) for 2 h and TOTO-3 (Invitrogen) for 10 min at room temperature. Images were obtained with a Zeiss LSM 510 Meta confocal microscope (Carl Zeiss).

Transactivation (coculture) Notch assay

One day prior to transfection, HeLa cells were seeded at a density of 5.0×10^4 cells per well in 12-well plate. Cells were transiently transfected with 1 μg of the pGL4-12xCSL-Luc reporter construct along with 0.05 μg of pGL4.74[hRluc/TK] (Promega) using Lipofectamine 2000 (Invitrogen). After 16 h transfection, medium was changed to 1:1 mixture of DMEM and EGM-2 and then 1.0×10^5 HUVECs were added. After adhesion of HUVECs (about 2 h later), cells were treated with or without 5 ng/ml BMP-9 for 24 h, and subjected to luciferase assay.

Statistical analysis

The difference between experimental groups of equal variance was analyzed using Student's *t*-test with $P < 0.05$ being considered significant. All experiments were performed at least three times independently and similar results were obtained.

RESULTS

Genome-wide identification and characterization of Smad1/5 binding sites in HUVECs and PASMCs

We performed ChIP-seq analyses using HUVECs stimulated with BMP-9 (1 ng/ml) or BMP-6 (50 ng/ml) and PASMCs treated with BMP-4 (50 ng/ml). Doses of the ligands for HUVECs were determined based on the phosphorylation status of BR-Smads and the physiological range of the circulating ligands. BMP-9 has been identified as a major circulating ligand for ALK-1 (27). Serum concentration of BMP-9 ranges from 1 to 12 ng/ml, which is enough for full activation of ALK-1 (Supplementary Figure S1A) (28,29). Thus, it is thought to play important roles in the control of vascular quiescence. BMP-6 transduces its signal mainly through the BMP type I receptor ALK-2 (encoded by *ACVR1*), which is also a receptor for BMP-9 (1). Notably, BMP-6 exists in FBS at concentrations of 2–10 ng/ml (29), and BMP-6 has been reported to activate ECs (30). However, 10 ng/ml was not enough to activate Smad1/5 in HUVECs (Supplementary Figure S1A). We selected a BMP-6 concentration of 50 ng/ml for our experiments, which gave an equivalent induction of *ID1* mRNA (Supplementary Figure S1B), and almost as high phospho-Smad1/5/8 level in the nuclear fraction as stimulation with 1 ng/ml BMP-9 (Supplementary Figure S1C). We also confirmed that 50 ng/ml BMP-4 was enough for full activation in PASMCs (Supplementary Figure S1D). Both HUVECs and PASMCs expressed Smad1 and Smad5 (Supplementary Figure S1E).

The anti-Smad1/5 antibody worked efficiently in IP under formalin-fixed condition (Supplementary Figure S1F and S1G). Human genomic DNA sequences that corresponded to known BMP responsive elements (BREs) in mouse *Id1* (12) and mouse *Hey1* (13) promoters were used as positive control regions. In HUVECs, a comparable enrichment of Smad1/5 was confirmed at the *ID1* promoter after BMP-6 or BMP-9 treatment, while weak Smad1/5 binding was observed at the *HEY1* promoter after BMP-6 stimulation (Supplementary Figure S1H). Since maximal Smad1/5 binding was observed at 1.5 h after stimulation with BMPs, we adopted this time of stimulation for ChIP-seq analyses, the same stimulation time that was used in similar studies of Smad2/3 (18) and Smad4 (31).

The ChIP DNA and the control input DNA were then submitted to high-throughput sequencing analyses. The enriched genomic regions were determined using CisGenome (19). Using a false discovery rate (FDR) cut off of 0.1, a total of 3750 Smad1/5 binding regions were identified in the ChIP-seq data of HUVECs treated with BMP-9, 880 in HUVECs treated with BMP-6 and 2745 in

PASMCs treated with BMP-4 (Figure 1A and B; Supplementary Figure S1I). To validate the results, BMP-9-dependent Smad1/5 enrichment was confirmed by ChIP–qPCR at 20 novel Smad1/5 binding regions of variable peak intensity (Figure 1C). The ChIP-seq peaks were annotated to a total of 2179, 563 and 1,609 genes, respectively (Supplementary Table S1). Approximately 30% of the binding sites were located in the introns of known genes and 20% in the promoter regions within 10 kb upstream of known transcription start sites (TSSs) (Figure 1D). These Smad1/5 binding regions were highly conserved among multiple vertebrate species (Supplementary Figure S1J).

Comparison of the three ChIP-seq data revealed that ~20% of Smad1/5 binding regions overlapped between HUVECs and PASMCs (Figure 2A), while most of the Smad1/5 binding sites in HUVECs after BMP-6 stimulation overlapped with those after BMP-9 stimulation, especially in the higher ranked peaks (Figure 2A and B). Common Smad1/5 binding sites shared with HUVECs treated with BMP-9 and those with BMP-6, including those at *ID1* and *ID3* loci, had comparable levels of Smad1/5 binding, suggesting that these sites had higher affinity for Smad1/5, while the BMP-9 specific sites (Figure 1A and B and Supplementary Figure S1I) had weaker affinity. In line with this hypothesis, increasing concentrations of BMP-6 dose dependently enhanced the Smad1/5 binding to the BMP-9 specific binding sites, e.g. at *HEY1* and *JAG1* loci (Figure 2C), whereas common Smad1/5 binding sites, e.g. at *ID1* and *ENG* loci, had enough enrichment when stimulated with only 20 ng/ml BMP-6 (Figure 2C). These dose response data also indicated that 50 ng/ml BMP-6 was not enough to achieve Smad1/5 binding to target sites with relatively lower affinity for Smad1/5 in ECs.

Smad1/5 bind to enhancer regions already accessible in specific cell types

To investigate the biological functions associated with Smad1/5 binding in HUVECs and PASMCs, the significance of functional annotation clustering of the GO of the genes related to Smad1/5 binding was assessed using DAVID (24). This analysis showed that the highest enriched GO category of biological function for HUVEC-specific genes with BMP-9 stimulation was related to blood vessel development, while that for PASMC-specific genes with BMP-4 stimulation was related to extracellular matrix production (Figure 3A). Thus, Smad1/5 bind to different sets of target sites in different cell types, which may be related to the cell type-specific function.

In order to identify the cell type-specific binding mechanism for Smad complex, we sought known binding motifs enriched in the Smad1/5 binding regions using the CEAS website (22). Interestingly, ETS, AP-1, AP-2 and SP-1 binding sites were enriched in the Smad1/5 binding regions in both HUVECs and PASMCs, while other motifs occurred only in a small proportion of sequences analyzed (Supplementary Table S3). We also conducted *de novo* motif prediction in order to find overrepresented motifs in the HUVEC- and PASMC-specific Smad1/5 binding regions using MEME (21). Obtained motifs were then compared with TRANSFAC (32) and JASPAR (20) database of known motifs, and ranked by their similarity using the TOMTOM program (33). The predicted motifs were similar to the ones identified by CEAS (Supplementary Figure S2). These results suggest that these transcription factors do not determine the cell type-specific BR-Smad binding pattern.

To evaluate the association between Smad1/5 binding and gene expression regulation, expression microarray analyses were performed at several time points (0, 2 and 24 h). We confirmed an equivalent induction of ID proteins after BMP-6 or BMP-9 stimulation in HUVECs (Supplementary Figure S3A). Combining the mapping data with gene expression profiles revealed that Smad1/5 binding regions were enriched in early upregulated genes (Figure 3B and C). Notably, in HUVECs treated with BMP-9, 108 genes were upregulated and 37 were downregulated more than 2-fold in early phase, and 70 of the 108 upregulated genes (64%) and 9 of the 37 downregulated genes (24%) were associated with Smad1/5 binding regions (Supplementary Figure S3B). We consider these 70 upregulated genes (corresponding to 170 binding sites) as putative direct target genes of ALK-1 in ECs (Supplementary Table S4). We also identified 19 putative direct target genes in PASMCs using the same criteria (Supplementary Table S4).

Smad1/5 binding regions in HUVECs were further characterized using differential histone modification marks, which were produced and released from the ENCODE Project (25). H3K4me3 is associated with promoters and H3K4me1 is preferentially associated with enhancers. H3K27ac is associated with active regulatory regions (34). As many as 3651 Smad1/5 binding peaks (97.4%) overlapped with H3K4me1 or H3K4me3 regions of HUVECs. Among them, 3201 Smad1/5 binding peaks (85.4%) overlapped with enhancer regions, characterized with both H3K4me1 and H3K27ac (Figure 3D and Supplementary Figure S3C) (34). In PASMCs, 86.5% (724/837) of common Smad1/5 binding peaks shared with HUVECs and PASMCs overlapped with enhancer regions of HUVECs characterized with both H3K4me1 and H3K27ac, while only 54.3% (1036/1908) of PASMC-specific peaks overlapped with endothelial enhancers (Figure 3D). Thus, these data also suggest that Smad1/5 preferentially bind to enhancer regions already accessible in specific cell types.

GC-SBE is a direct binding motif for Smad1/5

To elucidate a specific binding motif in Smad1/5 binding regions, a *de novo* motif prediction was performed using MEME (21). Since ChIP experiments may detect indirect Smad1/5-DNA binding through protein–protein interaction, we focused on the 170 Smad1/5 binding regions of BMP-9 target genes in HUVECs. Five overrepresented motifs were identified and designated as MEME1–5 (Figure 4A and Supplementary Figure S4A). These motifs were validated in three ways. First, the fold

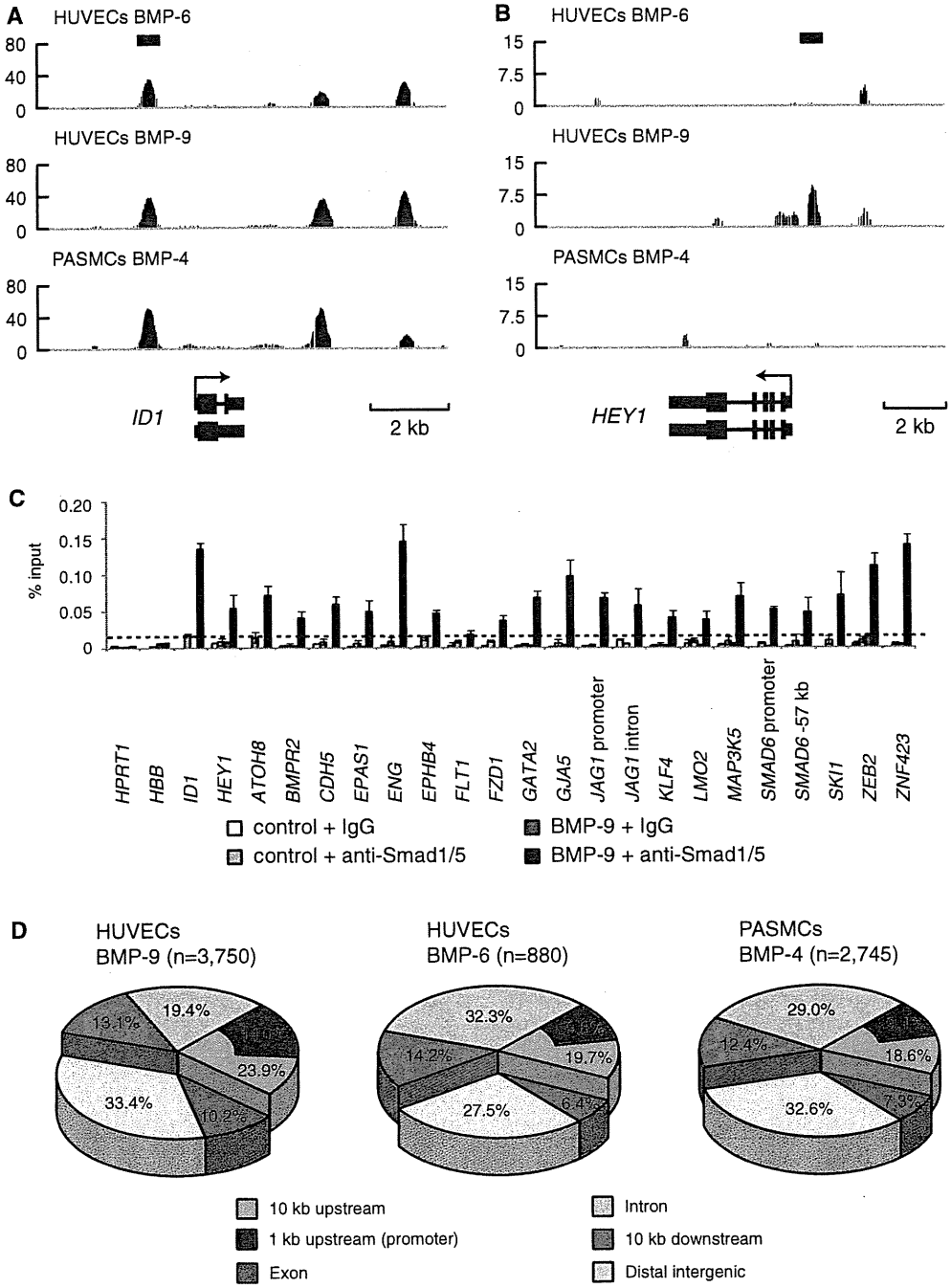

Figure 1. Genome-wide identification and characterization of Smad1/5 binding sites in HUVECs. (**A** and **B**) Genomic loci of *ID1* (A) and *HEY1* (B) are shown together with the results of ChIP-seq (in red). The direction of transcription is shown by the arrow beginning at the TSS. Horizontal black bars represent the positions of previously reported Smad1/5/8 binding regions. (**C**) HUVECs were stimulated with 1 ng/ml BMP-9 for 1.5 h and subjected to ChIP assays with anti-Smad1/5 antibody or control IgG. The ChIP samples were quantified by real-time PCR with locus specific primers and normalized to input DNA. The dashed line indicates 0.01% of input. The data are the mean of triplicate values ± SD. (**D**) Genome-wide location summary of Smad1/5 binding regions relative to known genes in human genome (hg18). Ten kilo base pairs upstream and downstream regions are defined as ≤10 kb upstream from the TSS or ≤10 kb downstream from the transcription end site (TES) of a gene, respectively. Distal intergenic refers to all locations outside the intragenic and the 10 kb flanking regions.

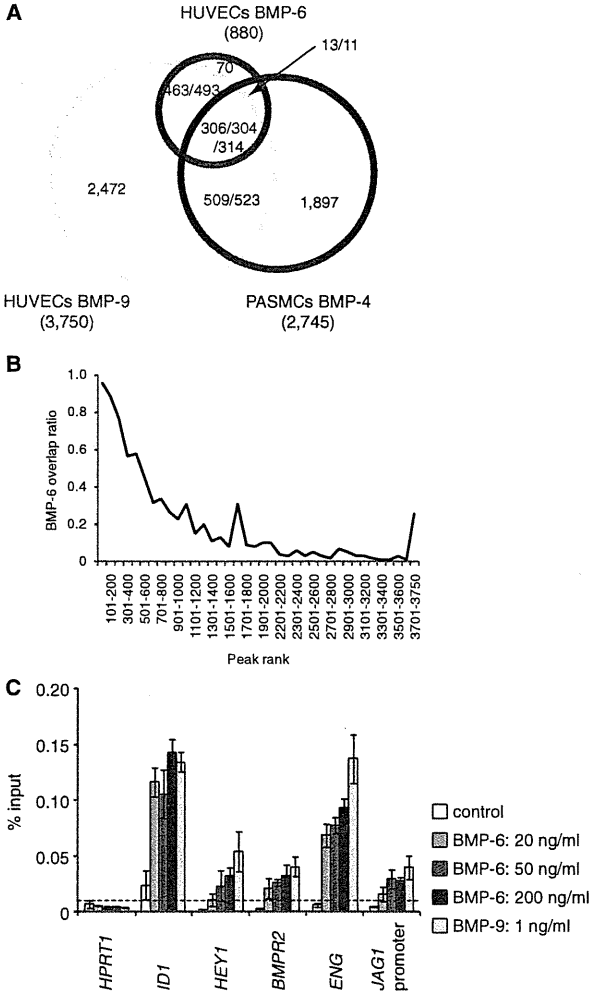

Figure 2. Comparison of Smad1/5 binding regions in HUVECs and PASMCs. (**A**) A Venn diagram represents the overlaps of Smad1/5 binding regions of HUVECs treated with BMP-9 (Yellow) or BMP-6 (Blue) and PASMCs treated with BMP-4 (Red). The number of binding regions of HUVECs treated with BMP-9 (Black) or BMP-6 (Blue) and that of PASMCs treated with BMP-4 (Red) are also shown. The numbers of overlapped regions are not identical, since some of the peaks are not on a one-by-one correspondence. (**B**) ChIP-seq peaks of HUVECs treated with BMP-9 are ranked by peak height. Fraction of peaks overlapped with the peaks of HUVECs treated with BMP-6 is calculated for every 100 peak and plotted. Overlapped peaks are enriched in the high ranked peaks. (**C**) HUVECs were starved overnight and stimulated with the indicated concentration of BMP-6 or BMP-9 for 1.5 h and were subjected to ChIP assays with anti-Smad1/5 antibody. The ChIP samples were quantified by real-time PCR with locus-specific primers and normalized to input DNA. The dashed line indicates 0.01% of input. The data are the mean of triplicate values ± SD.

enrichment of the motifs was compared (Figure 4B and Supplementary Figure S4B). Randomly selected genomic sequences (n = 1000) or non-overlapping matched regions (n = 50) were used as background controls. Four out of five motifs were significantly enriched in the Smad1/5 binding regions, and the MEME2 was the best. TFAP2A (also known as AP-2α) binding motif was a positive control and was found to be enriched in the Smad1/5 binding regions (Supplementary Table S3). No statistically significant differences were observed for motifs of transcription factors known to be expressed and functional in ECs, such as GATA2 (35). In contrast to the study of Chen and colleagues (16), the motifs for SOX2 and POU5F1 (also known as OCT4) were not enriched in the Smad1/5 binding regions, suggesting that different mechanisms or different enhancer complexes are adopted in differentiated ECs compared with mESCs. In addition, the incidence of the MEME motifs in the peaks was calculated. MEME2 occurred in about 45% of all Smad1/5 binding regions in HUVECs and PASMCs (Figure 4C and Supplementary Figure S4C). Moreover, it was enriched in the higher ranked peaks in HUVECs treated with BMP-9 (Supplementary Figure S4D). Finally, the relative distribution of the motif around the peak summits, where Smad1/5 was expected to be located, was analyzed. MEME2 was enriched in the Smad1/5 binding regions, especially around the peak summits, while other MEME motifs were not (Figure 4D and Supplementary Figure S4E and F). We therefore designated MEME2 as GC-SBE because it is similar in sequence to the previously reported GC-rich sequences for BR-Smads (11–13).

Analysis of the frequency of GC-SBE sequence in Smad1/5 binding regions revealed that GGCGCC sequence was enriched in Smad1/5 binding regions shared with HUVECs and PASMCs, while GGAGCC sequence was enriched in both HUVEC- and PASMC-specific binding regions (Figure 5A). To validate the enhancer activity of the Smad1/5 binding regions and the effects of the newly identified GC-SBE on the cell type specificity, luciferase assays were performed in HUVECs. Both *BMPR2* and *JAG1* were HUVEC-specific target genes (Supplementary Table S4). Fragments from Smad1/5 binding regions in intron 3 of *BMPR2* and the *JAG1* promoter, which contain the GGAGCC sequence, were cloned into a luciferase reporter construct (Supplementary Figure S5A). Both BMP-9 and BMP-6 were able to activate these reporters in HUVECs, while BMP-4 induced only weak response in PASMCs (Figure 5B and Supplementary Figure S5B and S5C). Consistent with ChIP data (Figure 1C), the Smad1/5 binding regions induced higher luciferase expression following treatment with BMP-9 compared with BMP-6. Even 1 ng/ml BMP-9 induced stronger luciferase activities in HUVECs than 50 or 200 ng/ml BMP-6 (Figure 5B). We also confirmed that these Smad1/5 binding fragments worked as transcriptional enhancers in the human microvascular endothelial cell line, HMEC-1 (Supplementary Figure S5D).

In order to compare the difference of enhancer activities between GGAGCC and GGCGCC sequence, a point mutation was introduced at the 'A' in the GGAGCC sequence. A mutation to GGCGCC induced higher luciferase expression compared with the GGAGCC wild-type. In contrast, a mutation to GGGGCC attenuated BMP responsiveness (Figure 5B and Supplementary Figure S5B). Interestingly, the fragments with GGAGCC